ANKARA YILDIRIM BEYAZIT UNIVERSITY

GRADUATE SCHOOL OF NATURAL AND APPLIED SCIENCES

DESIGN OF A MICROHEATER TO IMPROVE THE SENSITIVITY OF ELECTROCHEMICAL NUCLEIC ACID BIOSENSORS

M.Sc. Thesis by

İremnur AKÇAKOCA

Department of Material Engineering

December, 2020

ANKARA

DESIGN OF A MICROHEATER TO IMPROVE THE SENSITIVITY OF ELECTROCHEMICAL NUCLEIC ACID BIOSENSORS

A Thesis Submitted to

The Graduate School of Natural and Applied Sciences of

Ankara Yıldırım Beyazıt University

In Partial Fulfillment of the Requirements for the Degree of Master of Science in Material Engineering, Department of Material Engineering

by

İremnur AKÇAKOCA

December, 2020

ANKARA

M. Sc. THESIS EXAMINATION RESULT FORM

We have read the thesis entitled **"DESIGN OF A MICROHEATER TO IMPROVE THE SENSITIVITY OF ELECTROCHEMICAL NUCLEIC ACID BIOSENSORS"** completed by **İREMNUR AKÇAKOCA** under the supervision of **ASSIST. PROF. DR. FATMA DOĞAN GÜZEL** and we certify that in our opinion it is fully adequate, in scope and quality, as a thesis for the degree of Master of Science.

Assist. Prof. Dr. Fatma DOĞAN GÜZEL

Supervisor

Assist. Prof. Dr. Begüm ÜNVEROĞLU

Jury Member

Assist. Prof. Dr. Aligül BÜYÜKAKSOY

Jury Member

Prof. Dr. Ergün ERASLAN

Director

Graduate School of Natural and Applied Sciences

ETHICAL DECLARATION

I hereby declare that, in this thesis which has been prepared in accordance with the Thesis Writing Manual of Graduate School of Natural and Applied Sciences,

- All data, information, and documents are obtained in the framework of academic and ethical rules,
- All information, documents, and assessments are presented in accordance with scientific ethics and morals,
- All the materials that have been utilized are fully cited and referenced,
- No change has been made on the utilized materials,
- All the works presented are original,

and in any contrary case of the above statements, I accept to renounce all my legal rights.

Date: 30/12/2020 **Signature: ……...**

Name & Surname: İremnur Akçakoca

ACKNOWLEDGEMENTS

I would like to express my sincere gratitude to my advisor Dr. Fatma Doğan Güzel for the continuous support, providing me with the unique opportunity to work in the research area of Lab-on-chip technology, for her mentorship and encouragement.

I would like to thank, Dr. Hamed Ghorbanpoor, Dr. Araz Norouz Dizaji, Yasin Öztürk, Vahit Güzel, Dr. Ewen Blair and Dr. Damion Corrigan for their generous help for this research also for their friendship and companionship. I would like to also thank my family for their life-long love and support.

The research in this dissertation was supported by TUBITAK under Grant No: 217S793.

2020, December **İremnur AKÇAKOCA**

DESIGN OF A MICROHEATER TO IMPROVE THE SENSITIVITY OF ELECTROCHEMICAL NUCLEIC ACID BIOSENSORS

ABSTRACT

Electrochemical impedance spectroscopy (EIS) is often used for biomolecule detection based on the hybridization of the molecule onto the functionalized electrode surface and consequent impedance change. Though its performance is well established, there is still a need for improved sensitivity and specificity, especially when attempting to detect nucleic acids from clinical samples with minimal amplification steps. Localized heating is a potential approach for improving nucleic hybridization rates and reducing non-specific hybridization, and thereby producing high sensitivity and selectivity. The aim of the study was therefore to develop a microheater surrounding microeledtrodes, an integrated hybrid chip, sensing the genes of *Mycobacterium tuberculosis* with much higher sensitivity. The performance of the integrated hybrid chip was determined using the changes in the charge transfer resistance (R_{CT}) upon DNA hybridization using probe sequences for *Mycobacterium tuberculosis*. Heat transfer was simulated by using COMSOL Multiphysics as mathematical modeling. When the heat (50°C) was applied to the microheater during the DNA hybridization step, we observed that the R_{CT} values increased about 236% and 90% as opposed to on-chip heating experiments and off-chip non-heating experiments. We conclude from this observation that the microheater indeed can significantly improve the performance of the nucleic acid hybridization assay and paves the way for the development of highly- sensitive integrated label-free biosensors

Keywords: Electrochemical impedance spectroscopy, lab-on-a-chip, microheater, DNA hybridization sensitivity.

ELEKTROKİMYASAL NÜKLEİK ASİT BİYOSENSÖRLERİN HASSASİYETİNİ ARTIRMAK İÇİN BİR MİKRO ISITICI TASARIMI

ÖZ

Elektrokimyasal empedans spektroskopisi (EIS) biyosensörlerde ölçüm yöntemi olarak kullanılır. EIS yüksek performansa sahip bir ölçüm yöntemidir fakat özellikle nükleik asit biyosensörlerinde çalışılırken duyarlılığının ve özgüllüğünün geliştirilmesine hala ihtiyaç vardır. Nükleik asit hibridizasyonunun seçiciliğini arttırmak ve hibridizasyon oranını arttırmak için bölgesel ısıtma potansiyel bir yaklaşımdır. Çalışmanın amacı, elektrokimyasal sensör elektrotlarını çevreleyen mikroısıtıcı üretimi ve çalışma alanını sınırlandırmak için entegre edilmiş PDMS'in de bir parçası olduğu hibrit-çip üretimidir. Çip tasarımı hem ısıtma hem de nükleik asitlerin tespiti (çalışma ve karşı/referans) için elektrotlardan oluşmuştur ve AutoCAD yazılımı kullanılarak dizayn edilmiştir. Isı transferi ise COMSOL Multiphysics programı kullanılarak simüle edilmiştir. Hem mikro ısıtıcı hem de biyosensör elektrotları, gölge maskesi kullanılarak termal buharlaştırma yöntemi ile üretilmiştir ve mikro ısıtıcıların sıcaklık dağılımı termal kamera kullanılarak ölçülmüştür. Sensör elektrotlarının performansı, EIS ve Mycobacterium tuberculosis için prob dizileri kullanılarak DNA hibridizasyonu üzerine yük transfer direncindeki (R_{CT}) değişiklikler ölçülerek test edilmiştir. Sonuç olarak, DNA hibridizasyon aşamasında mikro ısıtıcıya ısı (50°C) uygulandığında, çip-içi ısıtma deneylerindeki R_{CT} değeri yaklaşık %236'lık artış gösterirken, çip-dışı sıcaklık olmadan yapılan deneylerdeki R_{CT} değerinin yaklaşık %90 arttığı gözlemlenmiştir. Bu gözlemden, mikro ısıtıcının gerçekten de nükleik asit hibridizasyon deneyinin performansını önemli ölçüde arttırdığı ve yüksek hassasiyetli entegre biyosensörlerin geliştirilmesinin yolunu açtığı sonucuna varılmıştır.

Anahtar Kelimeler: Elektrokimyasal empedans spektroskopisi, çipte laboratuvar, mikroısıtıcı, DNA hibridizasyon hassasiyeti.

CONTENTS

NOMENCLATURE

EIS	Electrochemical Impedance Spectroscopy
CV	Cyclic Voltammetry
DPV	Differential Pulse Voltammetry
SWV	Square Wave Voltammetry
Au	Gold
Cr	Chromium
R_{CT}	Charge Transfer Resistance
W	Warburg Impedance
R_s	Solution Resistance
C_{dl}	Double Layer Capacitance
Z	Impedance
V	Voltage
I	Current
W	Watt
SPEs	Screen Printed Electrodes
H_2SO_4	Sulfuric acid
DI	Deionized
PBS	Phoshphate Buffer Saline
TCEP	Tris(2-carboxyethyl)phosphine hydrochloride
MCP	3-mercapto-1-proponol
AFM	Atomic Force Microscopy
PDMS	Plexiglass
PMMA	Polydimethylsiloxane
C	Complementary
NC	Non-complementary

LIST OF TABLES

LIST OF FIGURES

CHAPTER 1

INTRODUCTION

Recently, the development of new reliable diagnostic methodologies has received a lot of attention. In this regard, biosensors are one of the ideal candidates for use at the point of care because of their capability to monitor and evaluate chemical and biological effects by producing signals either optical, electrical, or electrochemical [1-4]. Three important and essential components for a biosensor can be categorized as recognition, transduction, and signal processing.

Since biosensors offer many advantages as alternatives to conventional methods, they have been employed in many scientific and industrial areas such as chemistry, engineering [5], biology [6] by utilizing various types of bioreceptors like enzymes [7], cells [8], and aptamers [9].

Particularly, electrochemical impedance spectroscopy (EIS) can investigate in detail the relation between chemical and electrochemical effects via the passage of electric current between the solution and the electrode [10].

Electrochemical impedance-based DNA biosensors for nucleic acid hybridization are highly sensitive measurement tools, because, they are label-free possessing significant advantages such as not requiring extra assay steps or resources to label the target, making them lower cost, faster, and more portable over many labeled detection systems [11].

1.1 General View of Biosensor

The main purpose of a biosensor is to generate a signal that depends on the concentration of an analyte. The biosensor enables the analyte to be identified by chemical, physical, electrochemical, etc. signals and is used in many areas of science such as drug release, monitoring diseases, detecting nucleic acids, micro-organisms, as shown in Figure 1.1. Although the term of the biosensor was named by Camman in the 1960s, the first studies performed in the 1900s by M. Cremer. Clark and Lyons

pioneered the biosensor field and the first real biosensor was developed by Clark in 1956. The production of biosensors was commercialized in 1975 [12].

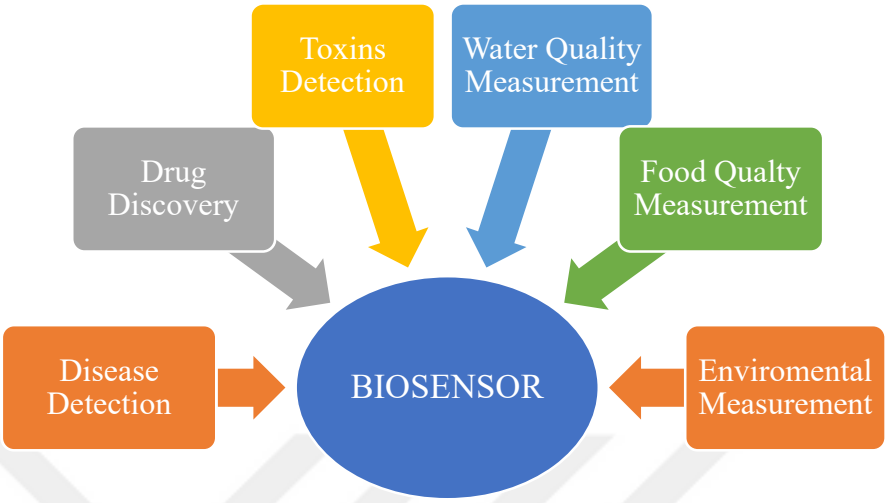

Figure 0.1 Biosensors using areas

1.1.1 Working Principle of Biosensor

A biosensor consists of different components, such as target, biorecognition molecules, transducer, and signal processing, as illustrated in Figure 1.2. The working principle of many biosensors is based on the fact that generally, the target interacts with biorecognition molecules, and the transducer senses this interaction producing a signal, thereafter the signal is transmitted to equipment that performs signal processing [13].

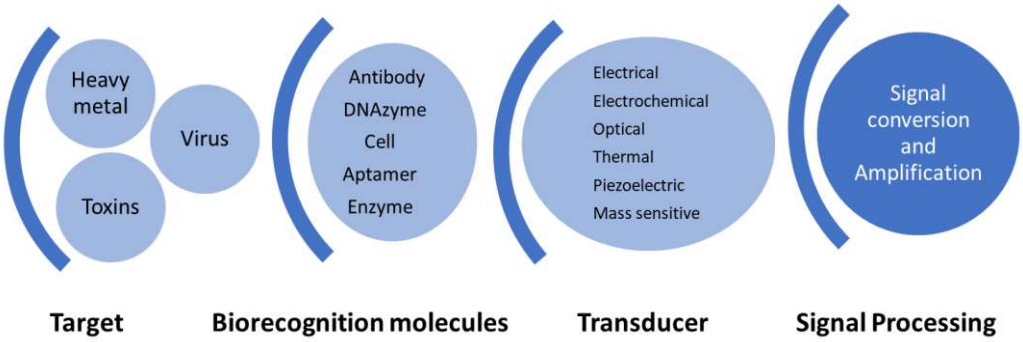

Figure 0.2 Different biosensor components

The basic components of a biosensor can be explained as follows:

a. Target: It is detected by a bioreceptor and can be heavy metal, virus, toxins.
b. Bioreceptor**:** Bioreceptor sends detectable signals to the transducer. Bioreceptor has to be specially recognized by the analyte of the interest such as cells, nucleic acids, aptamers, antibodies. The bioreceptor and transducer connect with various physical or chemical paths. The signals are transposed to the computer [14].
c. Transducer: In a biosensor, transducers are used to transform energy into different forms. It converts the signal generated as a result of the analyte-bioreceptor interaction into an energy form.
d. Electronics: This part processes the converted signal and prepares it for viewing, monitoring and/or analysis. This has a complicated electronic part that converts and duplicates analogs to digital form.
e. Display: It consists of software and hardware that produce results. The results can be an image, tabular, or graphic that can be changed according to user requirements [13].

1.1.2 Types of Biosensors

There are various types of biosensors such as optical and electrochemical biosensor [15].

1.1.2.1 *Optical Biosensors*

Optical biosensors provide various advantages in biosensor technology because optical biosensors have features such as desired harmless measurement and immediate results. Besides, they have the advantages of high precision measurements and an optimum measurement with a low amount of material. The optical biosensors technology has grown in the last ten years and different areas work with this type of biosensors [1].

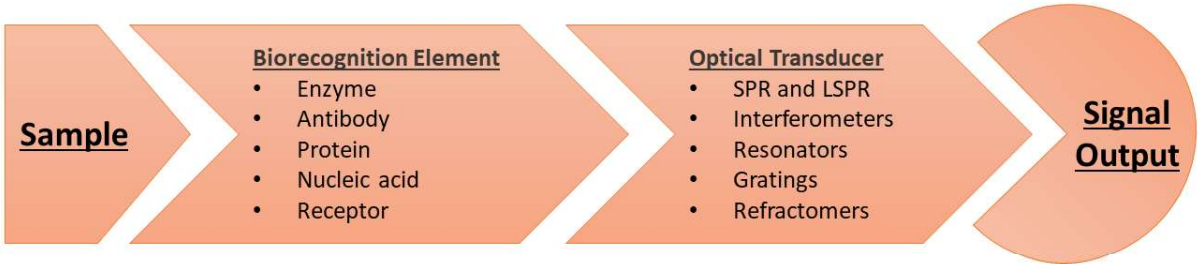

Figure 0.3 The general scheme of the working principle of optical biosensors

The optical biosensor has a transducer system that exhibits optical properties and it has a biorecognition element. Enzymes, antibodies, receptors, antigens, nucleic acids, etc. can be selected as the biorecognition element to be used in optical biosensors. Surface plasma resonance (SPR) and localized surface plasmon resonance (LSPR), interferometers, resonators, gratings, and refractometers are also used as an optical transducer, as shown in Figure 1.4 [16].

1.1.2.2 *Electrochemical Biosensors*

Electrochemical biosensors have electrochemical transducers and offer many advantages over optical biosensors such as label-free detection, low cost, portability.

Table 1.1 demonstrates the various electrochemical transducers and their measurement types [17].

Table 0.1 Types of electrochemical biosensors [17]

Type of measurement	**Transducer**	**Transducer analyte**
1. Potentiometric	-Ion-selective electrode -Glass electrode -Gas electrode -Metal electrode	-K^+, Cl^-, Ca^{2+}, F^- -H^+, Na^+ -CO_2, NH_3 -Redox species
2. Amperometric	-Metal or carbon electrode -Chemically modified electrode	-O_2, sugars -Alcohols, oligonucleotides
3. Conductometric, impedimetric	Interdigitated electrodes; metal electrode	Urea, charged species oligonucleotides…
4. Ion charge or field-effect	Ion-sensitive field-effect transistor (ISFET); enzyme FET (ENFET)	H^+, K^+ ……

Recently, electrochemical transducers have been used for the detection of DNA hybridization [18-20]. This electrochemical device has high sensitivity, offers the capability for portable detection and easy data acquisition, consumes minimum power energy. The general working principle is to detect the changing of current, as a result of Watson-Crick pairing [21].

The basic working principle of the detection using this type of sensors is as follows. Firstly, the electrode is coated with probe DNA, after immobilizing the probe to the electrode the target DNA solution is incubated over the electrode surface. Target DNA specifically matches the probe DNA (Figure 1.5). As a result of probe-target binding that is a hybrid duplex, the electron transfer at the surface of the electrode is affected. With the help of potentiostat, the current applied is measured in the form of resistance of the affected electron movement.

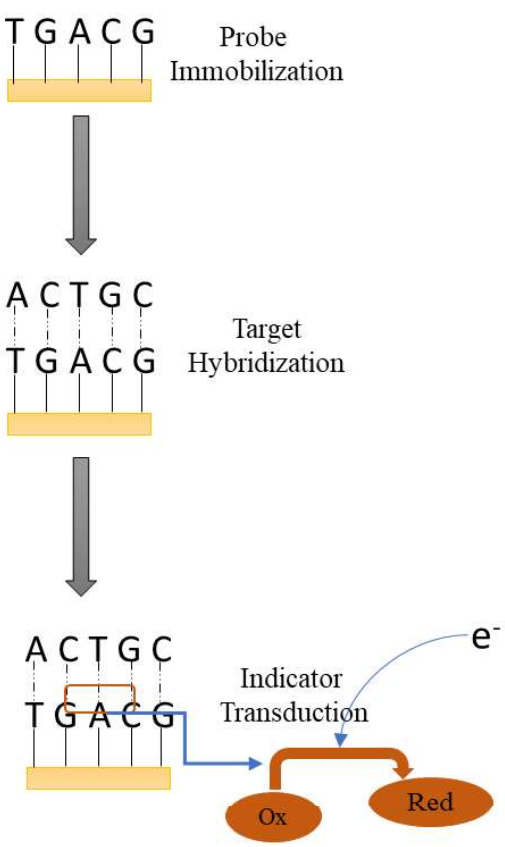

Figure 0.4 Basic principle of electrochemical nucleic acid biosensors

Within the scope of this thesis, in the next section, Electrochemical Impedance Spectroscopy (EIS) will be examined as one of the most common electrochemical biosensor platform.

1.1.2.2.1 Electrochemical Impedance Spectroscopy

Electrochemical impedance spectroscopy (EIS) was explored in the 1970s [22] but first using for a biosensor in the late 1980s [23], and its use has been increasing in recent years. It is based on the principle of impedance measurement by immobilizing the biorecognition molecule (aptamers, peptides, single-stranded DNA, etc.) on a specialized surface and then binding the analyte [24].

The impedance, symbolized as 'Z', comes from the methodology of detecting alternating current (I) as a result of applying a voltage (V) with a small amplitude. The impedance is formulated as follows [23]:

$$Z = \frac{V}{I} \tag{1.1}$$

In impedance, the alternating current does not only change in amplitude but also exhibit a phase shift (φ) according to the voltage change over time. Therefore, there is two part of impedance (Z): imaginary part (ZI) and the real part (ZR), as shown in Figure 1.6 [23].

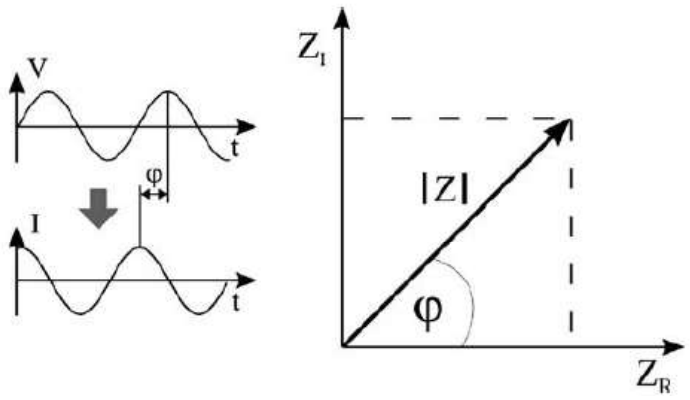

Figure 0.5 The impedance depends on voltage (time) and current (time) [23]

An interface which comprises electrode/electrolyte occurs at the electrode surface. Counter ions which are surrounded by solvent molecules achieve an electrical double layer (Cdl) at the electrode surface. Besides the electrode and electrolyte are in contact, the circuit forms solution resistance (Rs). The electron transfer from the electrode to the electrolyte is named charge transfer resistance (R_{CT}). With the increase of the negative charge, the charge transfer of negatively charged redox molecules was prevented in the solution which causes a change in the R_{CT}. The Warburg impedance (W) depends on the diffusion of mass transport and W increases at the low frequencies since reactants must diffuse far away (Figure 1.7a). Thus, impedance spectroscopy reveals a measurement method in which not only the characterization of layers but also diffusion processes can be detected.

An electrochemical impedance spectroscopy circuit uses ohmic resistance, Warburg impedance, constant phase element, and capacitance, as well as the electrolytic solution, as part of this measuring system. After the measurement, a Nyquist plot (Figure 1.7b) is obtained which comprises solution resistance (Rs), the double-layer capacitance (Cdl), the charge transfer resistance (R_{CT}), and the Warburg impedance (W), and expressed by Randles circuit, as shown in Figure 1.7a [11, 23]. A Nyquist plot consists of real and imaginary impedance axes and the frequency decreases to the right of the graph. At the beginning of the measurement, the solution resistance is plotted and then the impedance value begins to be recorded. Double-layer capacitance is calculated at the maximum point of the graph. The line obtained after the semicircle is also related to the Warburg impedance [23].

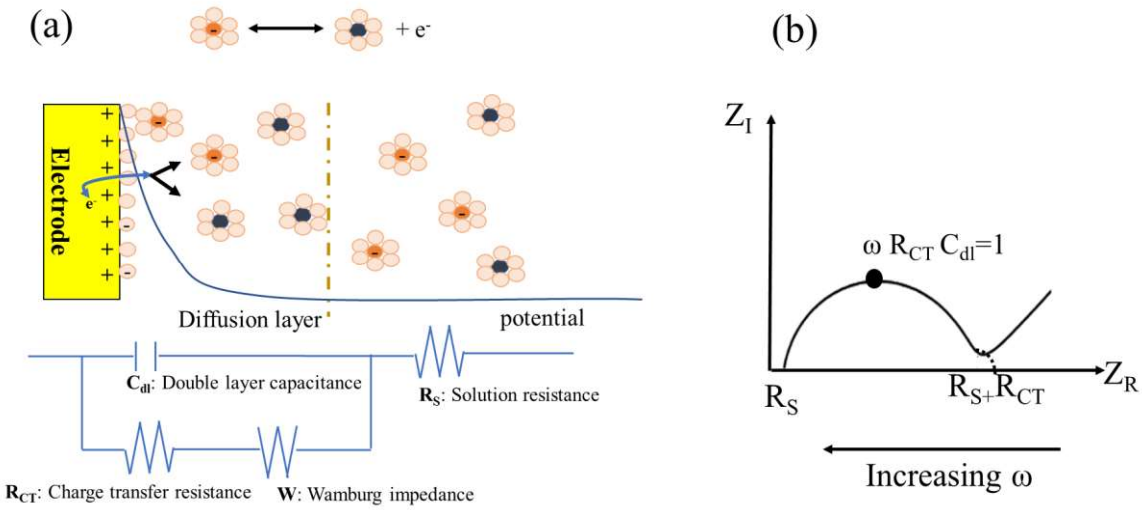

Figure 0.6 (a) The schematic illustration of the electrode/electrolyte interface and transforms to Randles circuit, (b) The Nyquist plot

The impedance spectroscopy system uses three different electrodes which are working, counter, and a reference electrode. The working electrode surface is immobilized by a biological sample such as nucleic acid. The working electrode controls the general impedance, so for this reason the counter electrode impedance should be fairly low. Since the impedance is inversely proportional to the surface area, the surface area of the counter electrode must be larger than the surface area of the working electrode. Besides, the electrolyte solution concentration used is calibrated between 0.01-1 M [25, 26].

Electrodes can be selected as to material properties such as electrical conductivity, durability, corrosion resistance, etc. Platinum, gold, graphite, etc. are used as counter electrodes, and Ag /AgCl or calomel electrodes are generally preferred as reference electrodes. The working electrode should be conductive and also can be selected as to the application area.

The most important and advantageous feature of EIS-based biosensors is that they are selective towards a particular interaction at the electrode-electrolyte interface. The perfect example is given from nucleic acid biosensors. The principle of this type of biosensors is based on the hybridization of a nucleic acid duplex. Simply, particularly nucleic acid sequence, also called probe DNA, as a bio-receptor are immobilized

electrode surface (gold, platinum, etc.). The electrode surface is used as a transducer component. A solution is prepared to connect the target DNA to the probe DNA which is first binding on the surface of the electrode and the target DNA is then selectively hybridized with probe DNA.

The sensitivity of the sensor can be enhanced when the electrode area is minimized while DNA hybridization selectivity can be increased through the imposition of elevated temperature, especially around the melting temperature of the DNA duplex [27, 28]. Microelectrodes which have been introduced recently, have highly advantageous properties over macro-electrodes. These features include low polarization time, low capacitance, low ohmic losses, and signal amplification [29].

Hybridization standard free energy is low at high-temperature and therefore mismatches can be minimized, the hybridization takes place more specifically at points close to the melting temperature [30]. The heat can be applied in different ways. In this study, a microheater was designed around a microelectrode in order to increase the sensitivity and selectivity of the sensor. In the next section, the features of microheaters will be examined.

1.2 Microheaters

A heater produces heat with resistance to the flow of electrons. The heat exchange can be controlled by applying a controlled voltage [31]. The typical heater is used for warming in the usual life or is used as a wire at the production of coil or cable. As for the micro-scale heater which is called microheater, the concept is the same but the effect of heat is used in various scientific areas such as gas sensors, biosensors, cell lysis, etc. to control of temperature. Two different types of microheater are emerging in microheater researches: thin film and wire heaters [32].

In the literature, various types of microheaters were designed to control temperature change such as meandered polysilicon made microheater on 2 μm thick S_iO_2 and 100, 200 nm thick Si_3N_4, polysilicon made microheater (S_iO_2, SiO_2/Si_3N_4, SiO_2/polysilicon), loop-shaped polysilicon made meandered heater ($SiO_2/Si_3N_4/SiO_2$) [21] and meandered platinum made microheater [31, 33, 34].

1.2.1 Performance Parameters of Microheater

There are several parameters that determines the performance properties of a microheater such as stability and robustness that is also an indicator of thermal and mechanical stress, distribution of stress. The relation between thermal stress and mechanical stress are parameters that determine whether the microheater is resistant to high operating temperature and long working times [35]. In addition heat response is important including such as accuracy, stability, response time, usage, accuracy, homogeneity, potential to use power, a lifetime. In the next sub-section, we will examine some of the parameters in detail.

1.2.1.1 *Thermal Loses*

Heat loss in microheater occurs as a result of radiation, conduction, and convection, however, the main decrease is caused by poor membrane conduction. An insulation layer can be used bottom and top the microheater to prevent heat loss [36], and also appropriate membrane can be selected as to convection, conduction, and radiation properties. Membrane heat loss can be expressed as [29, 37]:

$$Qtot = Conduction\ through\ membrane + conduction\ through\ air + radiation\ loss + convection\ loss$$

$$Q_{tot} = G_m\,\lambda_m\,(T_{hot} - T_{amb}) + G_{air}\,\lambda_{air}\,(T_{hot} - T_{amb}) + G_{rad}\,\sigma\varepsilon\,(T_{hot}^4 - T_{amb}^4) + \Delta x \quad \textbf{(1.2)}$$

Q_{tot}: Total heat loses

G_m, G_{air}, G_{rad}: The geometric factor because of the device design

T_{hot}: Active area temperature

T_{amb}: Environmental temperature

λ_m: Thermal conductivity of the membrane

λ_{air}: Thermal conductivity of air

ε: Emissivity

σ: Stefan-Boltzmann constant

1.2.1.2 *Heater Geometry*

Different microheaters are designed by researchers to achieve homogeneous temperature distribution [38-40]. There are three different methods for homogeneity which are to emplace a polysilicon layer below the microheater, to operate a metal alloy upside the microheater, and optimization of microheater geometry [35]. The different microheater designs are presented in this section, as a plane plate with a central hole, honeycomb shape, meander, S-shape, double spiral shape, and fan shape.

Plane plate with a central hole (Figure 1.9): This is a rectangular plate design with a central square hole. Its center causes natural convection. This structure has undistributed hot spots at the square hole and consumes high power.

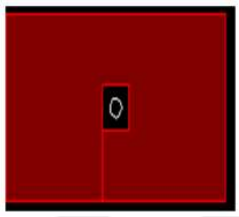

Figure 0.7 Plane plate with central hole microheater

Honeycomb shape (Figure 1.10): The temperature distribution is not homogeneous and the temperature difference between at the center and the corners is high [41].

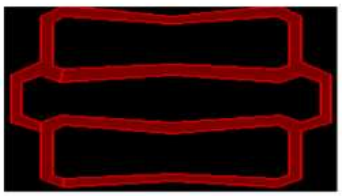

Figure 0.8 Honeycomb form microheater

Meander (Figure 1.11): The temperature distribution decreases homogeneously from the center to the corners [42], however, the temperature difference between the center and the corner is high due to design.

Figure 0.9 Meander form microheater

S-Shape (Figure 1.12): It is suitable for low power and homogeneous temperature profile and it can be an appropriate selection for small sizes.

Figure 0.10 S-form microheater

Double spiral shape (Figure 1.13): The design of a double spiral can be preferred in order to avoid the radial temperature gradient of the meander design,

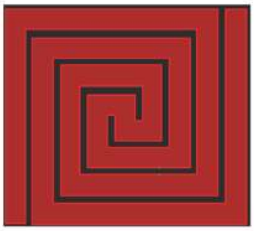

Figure 0.11 Double spiral form microheater

Fan shape (Figure 1.14): Fan shape microheater design is one of the best to provide less power consumption and a homogeneous temperature profile.

Figure 0.12 Fan form microheater [31]

1.2.1.3 *Temperature Distribution*

Temperature distribution varies according to the properties of the microheater. These properties differ as to the design and material selection, consequently, the distribution of temperature is controlled by a microheater. Based on microheater type such as meander non-uniform temperature distribution is revealed, and the maximum temperature is only observed in the center of the microheater. The homogeneity of temperature can be provided by using a double spiral form microheater [43].

Silicon which can be located at the bottom of the microheater can be used and homogeneous temperature distribution can be obtained because of the thermal conductivity properties [37, 44, 45], and glass, Si_3N_4, SiO_2, polyimide, ceramics can be also used [46, 47].

1.2.1.4 *Thermal Response Time*

A time period is defined as thermal response time that begins from the moment the power is applied to the microheater and passes until it reaches the stable temperature. Microheaters with low thermal resistance are preferred because their thermal response times are very short however, microheaters with low thermal conductivity consume high power [48].

1.2.1.5 *Mechanical Stability*

The difference between the thermal expansion coefficients, temperature gradients and time-dependent temperature changes of the materials used in micro heaters produces

thermal strain and stress [49], and also stress is observed in microheaters due to production errors.

When heat is applied to the material, its mechanical properties can change, so not every material with high electrical and thermal conductivity is used as a microheater. The mechanical properties of the material should be optimum at the temperature to be used. However, the membrane in which the microheater is produced has a low thermal conductivity to protect the heat. Si_3N_4 – SiO_2 composite ceramics have been used in the studies on the membrane. Stress is minimized as the compressive and tensile stresses of composite ceramics balance each other [50, 51]. Some electrothermal and mechanical properties for microheaters are summarized in Table 1.2.

Table 0.2 Significant properties of various microheaters [48]

Materials	**Membrane Material and Structure**	**Heater Geometry**	**Max. Temp.**	**Power Consumption**
Al	Glass	Irregular shaped meander	140°C	-1000mW
Au/Ti	Pyrex7740	Meander	164°C - 300°C	50mW- 100mW
Cr	SiO_2/ Si_3N_4 Membrane	N. S.	130°C	N. S.
Pt	Si_3N_4 Membrane	N. S.	500°C	250mW
	Si_3N_4 plug, Membrane	N. S.	170°C	75mW
	Si_3N_4 plug, Membrane	N. S.	300°C	75mW
	Si_3N_4/SiC, suspended Membrane/ Microbridge	Meander	700°C	9.25mW
	SiO_2/ SiC, suspended Membrane/ Microbridge	Irregular	870°C	300mW
	SiO_2/ Si_3N_4, 3D suspended Membrane/ Microbridge	3D Meander	400°C	20mW
	Porous Silicon, suspended Membrane/ Microbridge	Meander	600°C	33mW
Pt:Si	Si, suspended membrane/ Microbridge	Meander	400°C	500mW

Pt/Ti	SiO_2, suspended Membrane/ Microbridge	Meander	400°C	9mW
	SiO_2/ Si, suspended Membrane/ Microbridge	Meander	350°C	60mW
Poly Silicon	SiO_2/ Si_3N_4, suspended Membrane/ Microbridge	N. S.	500°C	68mW
	SiO_2, suspended Membrane/ Microbridge	Meander	300°C	12mW
	Si_2N_2O, Membrane	Square with center hole	420°C	65mW
	SiO_2/ Si_3N_4, Membrane	Meander in a loop	600°C	50mW
SiC	SiC, Microbridge	Square	300°C	8.6mW
Ni	SiO_2/Si, Membrane	Meander	250°C	120mW
NiFe	Silicon oxynitride, Membrane	Meander	300°C	55mW
HfB_2	SiC, Suspended membrane/ Microbridge	N. S.	380°C	35mW
	SiC, Suspended membrane/ Microbridge	N. S.	250°C	20mW
Mo	SiO_2/ Si_3N_4, Membrane	Double Spiral with rounded corner	850°C	86,4mW
TiN	Si_3N_4, Membrane	Double Spiral with rounded corner	700°C	~85mW
W	SiO_2/ Si_3N_4, Membrane	Circular	300°C	6mW
Si:B	Si, suspended Membrane/ Microbridge	Meander with corner	1000°C	500mW

*N.S.:Non standart

1.2.2 Materials Selection and Fabrication for Microheater

The processing method and the properties of materials affect the microheater quality. Generally, a microheater consists of an insulating and a resistive layer. The insulation layer is below the resistive layer, and the resistive layer is the main source of heating. Mostly glass [32], silicon [52], ceramics [53] or stainless still [34] are used for insulation layer materials. Silicon and ceramics can be used to provide a wide temperature range than glass and steel [38]. Silicon with high thermal conductivity is used at high temperatures (1000°C) [52]. Alumina has a high thermal conductivity

which is caused by the consumption of high power while ceramic and glass create lower conductivity and consume lower power [53]. Stainless still has some beneficial properties that are robust, inert, easy to produce in terms of microfabrication, and high thermal conductivity.

A microheater has the capacity of heating up to tens of milliseconds in a short time. The electrically conducting heating layer can be metal-ceramic or doped polysilicon. Metal provides high heat efficiency with low voltage and ceramic can be preferred because of reactivity [47]. Metal is the most preferred heater material in the literature because the metal is easy to be designed, temperature control is simple [32]. In addition to these positive features, the most important negative feature is inertness but the inert property can be easily handled with the insulation layer [35].

In general, platinum is used as microheater material due to its high electrical and thermal conductivity, inertness, high melting point, as shown in Table 1.3. Platinum can be used at over 500°C and resists oxidation [36]. Silver is more conductive compared to platinum however, it is more reactive and can become tarnished over time.

Gold is the other microheater materials [15] and the properties required in an electrode material are conductivity, reactivity, malleability, and cost. Because of these characteristics, gold can be preferred as microheater materials [31].

Table 0.3 Significant properties of various microheater materials [35]

Material	**Electrical resistivity Ωm**	**Temperature coefficient of resistance 10^{-3} K^{-1}**	**Melting point °C**	**Thermal conductivity $Wm^{-1}K^{-1}$**	**Tensile strength MPa**	**Young's modulus GPa**
Pt	$10.6x10^{-8}$	3.9	1772	71.6	145	171
Al	$2.65x10^{-8}$	3.9	660	237	45	62
Cr	$12.5x10^{-8}$	2.9	1845	94	83	248
Au	$2.35x10^{-8}$	3.4	1063	318	103	78
Mo	$5.2x10^{-8}$	5.1	2621	138	450	325
Ta	$12.45x10^{-8}$	3.8	2996	54	220	186
Ti	$54.3x10^{-8}$	3.8	1680	21.9	235	1111

Besides the material type, the type of microheater is also an important factor. In the literature, microheater types have been examined in two groups: Wire and thin film [35].

1.2.2.1 *Types of Wire Microheater*

Table 1.3 lists the properties of microheater materials. It is very useful to examine the material properties in this way to choose the appropriate microheater material. Depending on the material purity and production method, the values in the table can be varied. Besides, when working at high temperatures and thin films, the material properties can vary greatly [54] [32].

1.2.2.2 *Types of Thin-film Microheater*

Thin-film microheaters have less heat loss than wire heaters and can be integrated more easily. At the same time, it has fast heating, conservation of temperature, and low power consumption features. Besides, production techniques have a significant effect on the crystal structure, grain size, and density of the material. This contributes to optimizing the material properties according to applied science such as biosensor, gas sensor, MEMS device, etc.

Recently microheater platforms have been used in significant areas of applied science. Kathirvelan *et al.,* studied platinum microheater on the silicon substrate, reached 300 K to 1200 K temperature for sensor applications. 0.5 V and 4 V was applied to achieve the desired temperature and the microheater was characterized with the finite element method [39]. Velmathi *et al.* tried to optimize thermal management of microheater and COMSOL was performed to characterize temperature distribution of different design of microheater. Double spiral, S-shape, fan type with a size of 500 μm and 500 μm were tested and related temperature distributions were shown [31].

Sidek *et al.,* characterized microheater geometries which were meander, parallel, and double meander. In this study, platinum was the preferred heating element. The simulation was performed by Conventor Ware Process Editor and also electrical

potential, current density was examined [40]. Chang *et al.,* produced a multilayer microheater from chromium-chromium nitride and chromium nitride-platinum using MEMS technology. Duration time and maximum heat temperature were characterized by applying various voltages [36].

Zhang *et al.,* fabricated a thin microheater from gold/titanium by using photolithography and electro-thermal simulation was performed using finite element software ANSYS [32]. Ha *et al.,* manufactured a microheater- microfluidic platform to perform thermal cell lysis. Microheater temperature was increased to 80°C to lysis human buccal epithelial cells and microheater was fabricated using with thermal evaporator method: Firstly 20 nm chromium layer was deposited as an adhesion layer and then 100 nm gold as heater layer [55].

Li *et al.,* utilized polydimethylsiloxane (PDMS) integrated microheater for the application of polymerase chain reaction (PCR). Three temperature interval which are 90°C -95°C, 50°C-65°C, and 70°C-77°C were aimed in this study and three different microheaters were fabricated to apply temperature. PDMS and microheater were produced photolithography and integrated by reactive ion etching (RIE)-plasma bonding [56].

Nieto *et al.,* fabricated an aluminum microheater to perform cell culture on the chip and used the laser microfabrication technique for production [57]. Javed *et al.,* produced a platinum microheater on a glass substrate by photolithography for the detection of temperature-dependent DNA binding interactions. The finite element method was performed to characterize temperature performance and fluorescent images were recorded to detect microheater performance [58]. In another study, DNA hybridization specificity was increased just below the melting temperature of DNA since the hybridization standard free energy is low at high temperatures [30].

1.3 Motivation and Objectives

Electrochemical Impedance Spectroscopy (EIS) is a highly sensitive tool and is mostly used in biosensors. Impedance is similar to resistance but has a frequency dependence in which the impedance response of an electrochemical reaction typically consists of

double-layer capacitance, solution resistance, Warburg impedance, and charge transfer resistance. It is modeled as an electrical circuit called the Randles equivalent circuit. When electron transfer begins, as a result of an electrochemical reaction, the resistance of this process is called charge transfer resistance (R_{CT}) and is commonly used in biosensor measurements to determine whether the bioreceptors on the surface have successfully bound to their target [23, 24, 25].

DNA hybridization specificity can be increased through the imposition of elevated temperature, especially around the melting temperature (T_M) of the DNA duplex. Hybridization standard free energy is low at high-temperature and therefore mismatches can be minimized [27, 28, 30].

The goal of this study was to produce a simple planar chip bearing gold electrodes which were successfully used to detect specific DNA hybridization. The design and incorporation of electrodes provided an opportunity to exert control over temperature for improving assay sensitivity and specificity.

The results presented here showed the initial modeling and fabrication of highly-sensitive integrated label-free biosensors, followed by characterization of the assay performance on the system with comparison to a benchmark electrode model.

CHAPTER 2

EXPERIMENTAL PART

2.1 Design and Simulation

A hybrid-chip was designed to include both Au-made microelectrodes for heating and measuring impedance using AutoCAD software. Heat transfer was then simulated with mathematical modeling by using COMSOL Multiphysics.

2.1.1 Design of the Hybrid-chip with AutoCAD Software

The microheater and the microelectrodes were designed using AutoCAD software. Firstly, the glass slide of 26 mm by 26 mm was depicted on the software and then the microheater and microelectrodes were located over the glass slide.

Figure 2.1a demonstrates the glass slide, the microheater, and the microelectrode. The working electrode (WE) and counter/reference electrodes (CE) are shown in Figure 2.1b while Figure 2.1c demonstrates designing a microheater platform. The width of CE and WE is 1 mm and 0.2 mm, respectively. The width of the contact pads is 4 mm while the length between WE and CE is 4 mm. The width of the microheater channel is 0.2 mm and the width of the contact pad is 4 mm.

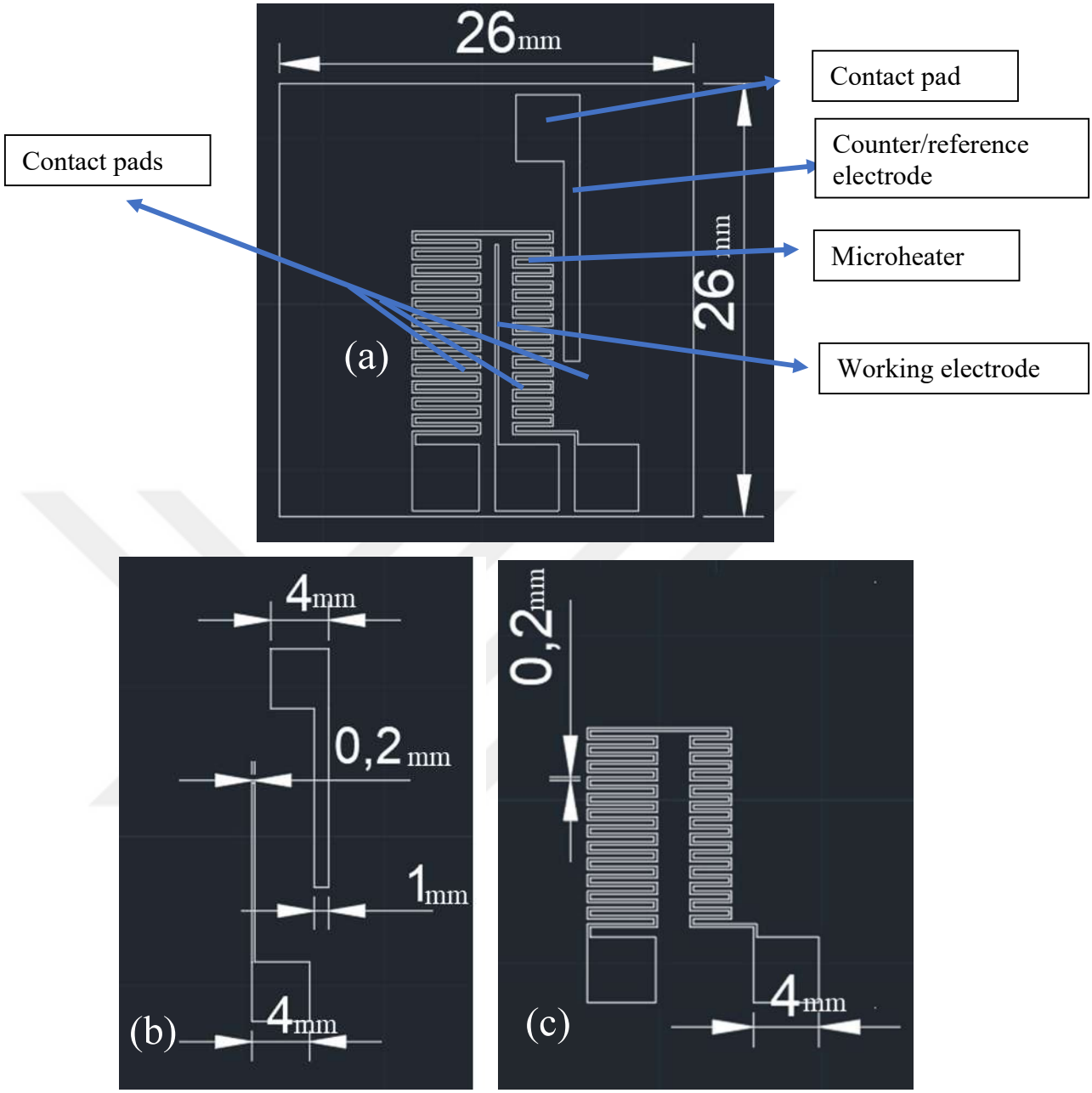

Figure 0.1 (a) Design of the hybrid chip, (b) Design of WE and CE, and (c) Design of microheater and contact pads

2.1.2 Heat Transfer Simulation

AutoCAD drawing of the hybrid-chip was transferred to the COMSOL Multiphysics software. As a start, AutoCAD drawing was simulated to obtain suitable temperature in the microheater. Heat transfer modulus was applied to determine the suitable power and temperature distribution. Therefore, simulation for heat transfer was carried out

using thermal expansion, temperature coupling, and electromagnetic heating multi-physics. A potential of 3.2 W was applied and as a result, the microheater surface temperature increased to 50°C.

2.2 AFM Characterization of Electrodes

Atomic Force Microscopy (AFM) (Quesant Q-Scope 250, Euromex, Nederlands) was operated for the characterization of the morphology of electrode surfaces [19]. SPE and hybrid-chip were cleaned with DI water for 10 seconds, dried with nitrogen, and scanned an area of 49 μm by 49 μm with AFM.

2.3 Production of the Chip

Shadow mask was produced from aluminum by Photofab (Cambridge, UK). The integrated hybrid-chip was fabricated on 26 mm by 26 mm glass slides. by thermal evaporation. Glass slides and shadow mask were cleaned with acetone and then dried with nitrogen gas. Initially, 100 nm of chromium (Cr) (99.99%) (Nanovak, Turkey) was deposited to form an adhesion layer between glass and gold (Figure 2.2a-II). 300 nm of gold (Au) (99.99%) (Nanovak, Turkey) was then deposited on the adhesion layer, as shown in Figure 2.2a-III. The deposition was performed through the shadow mask using a thermal evaporator at Bilkent University (UNAM) (Figure 2.2a-I). After the removal of the shadow mask, the final chip was obtained, as shown in Figure 2.2a-IV. A photography image of the fabricated hybrid-chip is shown in Figure 2.2b.

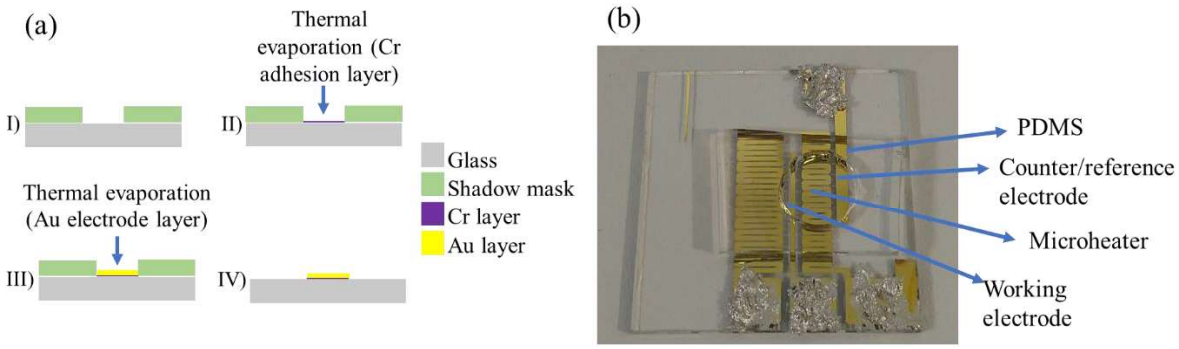

Figure 0.2 Schematic illustration of the fabrication procedure; (a) Hybrid-chip production process (I, II, III, IV), (b) Photography image of the manufactured hybrid-chip

2.3.1 Electrochemical Impedance Spectroscopy Experiments

The CV cleaning proceeded between -0.5 V and 1.75 V until the peaks which were oxidation and reduction, were not switching and after this to determine the cleaning characterization, the electrodes were cycled with CV in the 1 mM ferri/ferrocyanide. CV was characterized to determine peak-to-peak separation between -0.25 V and 0.5 V and EIS results were recorded as charge transfer resistance (R_{CT}). The R_{CT} values were performed pre probe, post probe, and post target measurement in a 1 mM ferri/ferrocyanide solution. The EIS frequencies were changed between 100 kHz and 0.1 Hz.

EIS experiments were divided into two-part:

a. **Off-chip experiments:** Macro-gold electrode (Figure 2.3a) and C223AT screen-printed electrodes (SPEs) (Metrohm, Switzerland) (Figure 2.3b) were used. Heating was performed using a commercial incubator.
b. **On-chip experiments:** The designed hybrid chip was used. Heating was performed using the microheater.

Each part includes heating and non-heating experiments.

2.3.1.1 Off-chip Experiments

2.3.1.1.1 Off-chip Experiments Non-heating

This experiment was partially conducted at the University of Strathclyde, UK, in collaboration with Dr. Damion Corrigan. Initially, the optimization of DNA hybridization protocol was practiced using a macro-gold electrode. Following experiments were carried out using C223AT SPEs.

Figure 0.3 The used electrodes (a) macro-gold electrode, (b) C223AT SPE

The experiment consists of four steps, as previously described by *Blair et al.,[26]*. Before the cleaning step, the macro-gold electrode was cleaned with a piranha solution (75% H_2SO_4 and 25% H_2O_2, Sigma Aldrich, USA), because a macro-gold electrode could be used couple of times as distinct from SPEs. Oligonucleotides were purchased from Sigma Aldrich (USA), the sequences are shown in Table 2.1. Probe and target sequences were received from Dr. Damion and Dr. Ewen in UK. In the next section, we will describe the protocol for electrochemistry experiments.

Table 0.1 DNA sequences used for the experiment

Function	**Sequence**
Probe	CCACAAGACATGCATCCCG
Complementary Target	CGGGATGCATGTCTTGTGT
Non-complementary Target	GTCTTCTTGGCGACCTCTTT

1. Cleaning step: Electrodes were rinsed with deionized (DI) water and was cycled in the solution of 0.1 M H_2SO_4 (sulfuric acid) using cyclic voltammetry (CV) between -0.5 V to 1.75 V until graph unchanging. The electrode connections were made using a commercially available electrode holder (DropSens, Methorm, Spain).

2. Pre probe measurement: After the CV cleaning, the electrodes were rinsed DI water for 10 sec and CV, Differential Pulse Voltammetry (DPV), Square Wave Voltammetry (SWV), EIS (100 kHz and 0.1 Hz) were performed in the solution of 1 mM ferri/ferrocyanide (Sigma Aldrich, USA) using PalmSens-P4 potentiostat (PalmSens, Houten, Netherlands). The electrode was then incubated 16-24h in room temperature with 3 μM probe DNA (15 μM TCEP (Tris(2-carboxyethyl)phosphine hydrochloride) and 1xPBS (phosphate saline buffer) (Sigma Aldrich, USA) solution inside of a container, as shown in Figure 2.4b.

The last incubation for this stage was with 3-mercapto-1-propanol (MCP) (Sigma Aldrich, USA) solution which was prepared using 1 mM MCP, 5 mM TCEP, and 1xPBS was backfilled on the gold electrode surface which was already immobilized with probe DNA.

3. Post probe measurement: After rinsing electrodes with DI water in 10 sec, DPV, SWV, EIS were measured in the 1 mM ferri/ferrocyanide solution, and electrodes were incubated for 1 hour, with 500 nM target DNA solution.

4. Post target measurement: Electrode was rinsed with 0.05 % PBS in 20 sec, dried with a wipe, and post target measurements of DPV, SWV, EIS were performed in the 1 mM ferri/ferrocyanide. The experimental steps are illustrated in Figure 2.4a.

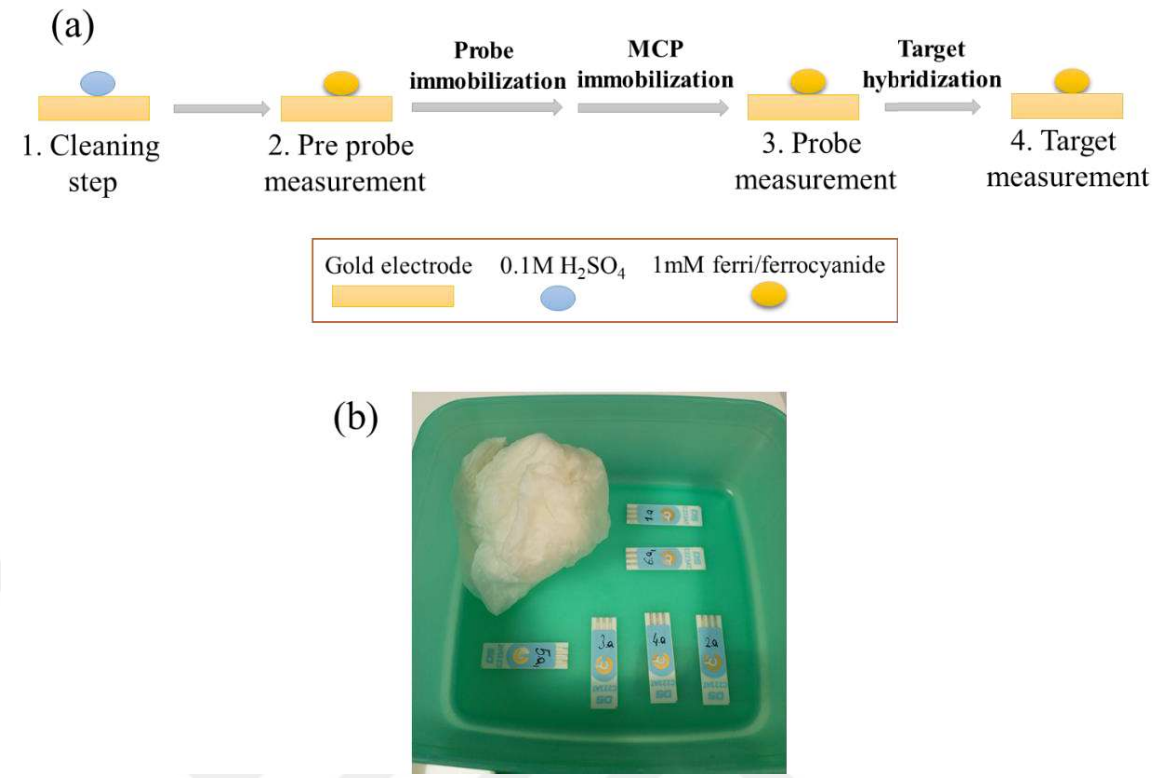

Figure 0.4 (a) Schematic illustration of experimental steps, (b) The pictures of the incubation container

2.3.1.1.2 Off-chip Experiment With Heating

The on-chip experiment was also conducted using the same protocol. However, C223AT SPEs were only used in this step.

The off-chip experimental setup using the SPEs is shown in Figure 2.5. Target incubation was performed in the incubator (JSR, Korean) to increase hybridization temperature to 50°C.

Figure 0.5 The off-chip experimental setup

2.3.1.2 On-chip Experiments

A PDMS slab with a mm size aperture was bonded using plasma onto the microheater and Au-made microelectrodes in order to limit the working area, as shown in Figure 2.6a. To ease the handling of the chip and provide an efficient connection between the Au-made microelectrodes/microheater contact pad and the power supply/PalmSens, a specific chip holder entitled jig was designed and manufactured from plexiglass (PMMA), as shown in Figure 2.6b. The jig was designed by Yasin Öztürk and produced by Yasin Öztürk and Vahit Güzel in Pleksiart (Turkey).

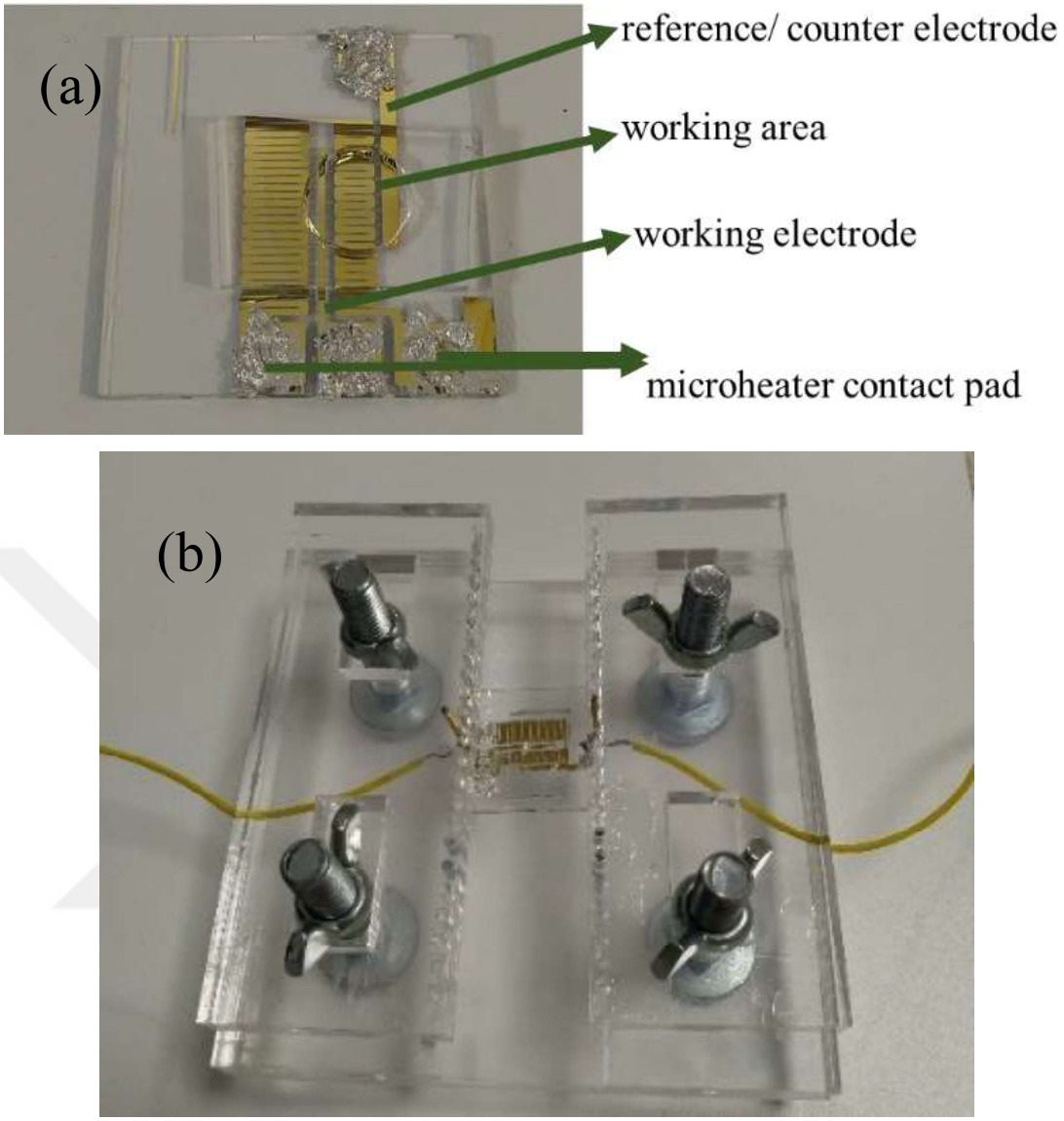

Figure 0.6 (a) Fabricated hybrid-chip, (b) Hybrid-chip with the produced jig

2.3.1.2.1 On-chip Experiment Non-heating

The above-mentioned protocol was also applied for on-chip experiments. Conductive epoxy (ElTech 235, Pulsar, Turkey) was applied over the contact pads of electrodes to increase the quality of the connection, and pins (Çalışkanlar A.Ş) were used for the PalmSens connection. Cables were placed on the edge of the pins to easy control the connection. The pins which were already emplaced inside of the jig were aligned over the contact pads, and the crocodiles of PalmSense were connected to the jig cables.

2.3.1.2.2 On-chip Experiment With Heating

The experimental protocol is the same as above. However the heat was provided using the microheater when the power was applied to the microheater. Figure 2.7 illustrates the experimental setup.

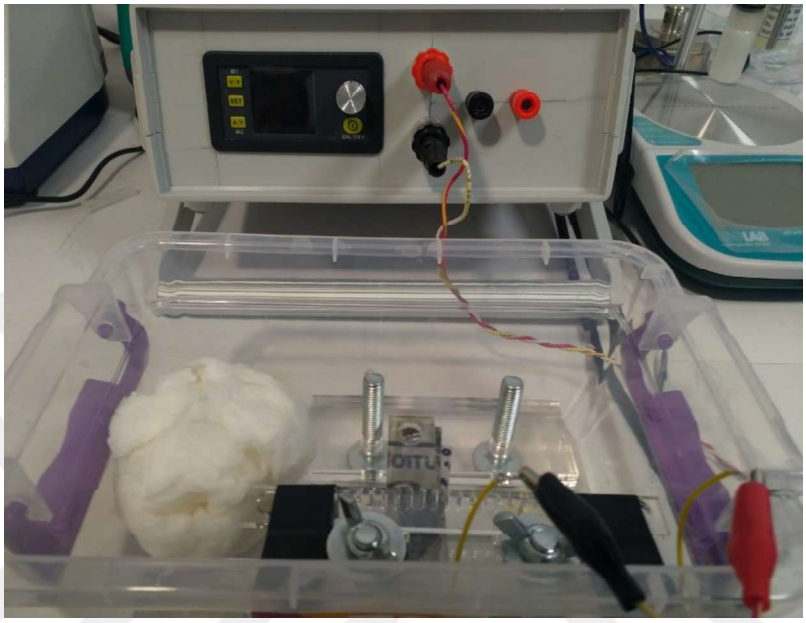

Figure 0.7 The on-chip heating experimental setup.

CHAPTER 3

RESULTS AND DISCUSSION

The aim of this study was to design a microheater and investigate the effect of the use of the microheater in EIS experiments. The function of the heater is to reach the desired temperature and maintain this temperature. 50°C, which is close to the melting temperature of the target, was used to minimize non-specific DNA-DNA interactions [30, 59]. Besides the microheater, microelectrodes which have specific properties such as low polarization time, low noise, low capacitance, etc, were also operated [29].

3.1 Characterization of Microheater Performance

As a result of the simulation, the temperature in the center of the microheater reached 50°C in approximately 1 minute, when 0.32 W was applied. It has been observed that the temperature decreases homogeneously towards the edges of the glass slide starting from the center. The temperature difference between the center and the corners is about 10°C. Figure 3.1 demonstrates homogeneous temperature distribution when applying 3.2 W.

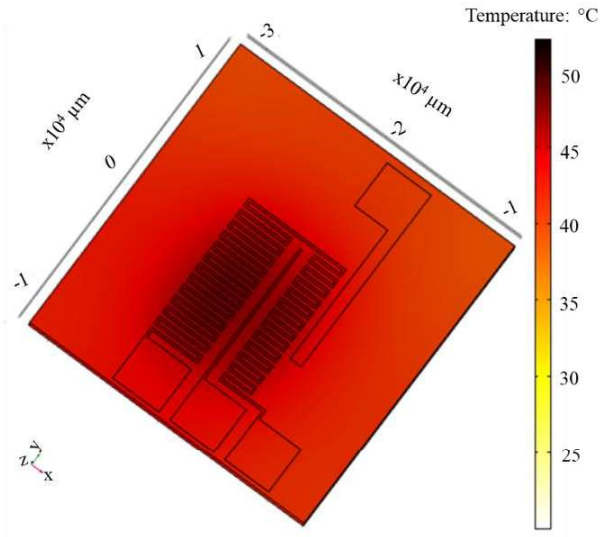

Figure 0.1 Homogenous temperature distribution of designed microheater

The experimental heat transfer data obtained using the thermal camera (Fluke, USA) is illustrated in Figure 3.2a. As seen in the figure, the heat generated around the WE is homogenous and the temperature was achieved to 50°C when 0.3 W was applied from the power supply. The temperature difference between the center and the corners of the microheater was about 10°C, and this result supports the simulation.

When the maximum power of 1.68 W was applied, temperature of 158°C was obtained and the microheater was fractured (Figure 3.2b). Apart from this observation, all the tests were performed successfully.

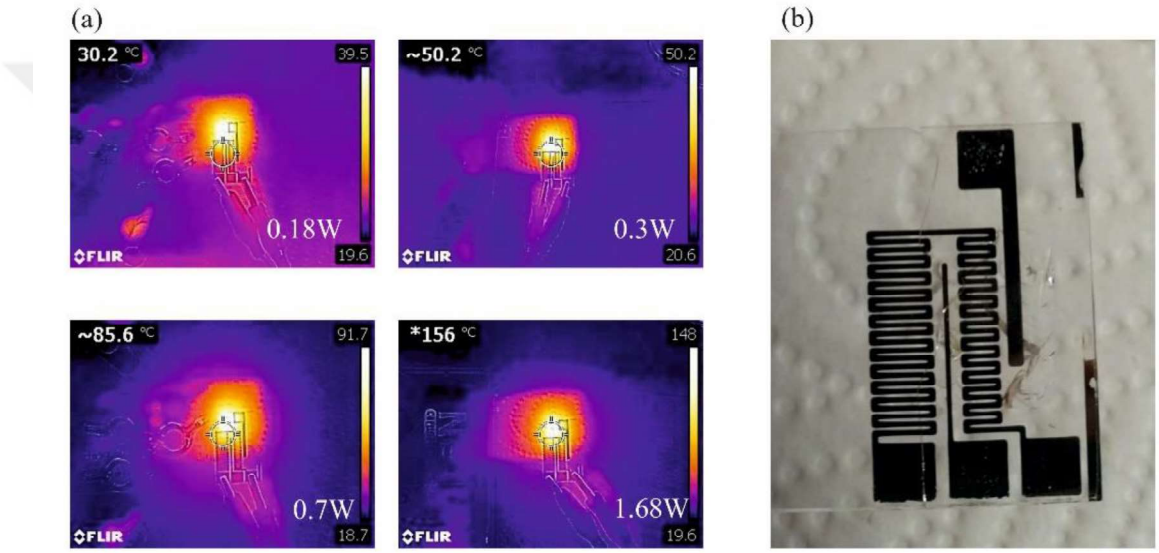

Figure 0.2 (a) The power-temperature performance of microheater: 0.18W-30.2°C; 0.3W-50.2°C; 0.7W-85.6°C; 1.68W-156°C, (b) the cracked view of microheater

In light of the simulations and initial observations, different power values and durations were tested in order to monitor and optimize the heat generation, as listed in Table 3.1 and Table 3.2, graphed in Figure 3.3 a and Figure 3.3 b.

Table 0.1 Temperature changes with power (watt)

Temperature (°C)	30	40	50	70	90	110	130	158
Power (W)	0.06	0.18	0.3	0.52	0.7	1	1.4	1.68

Table 0.2 Temperature changes with time (minute)

Temperature (°C)	42	50.8	54.5	56.9	58	59.1	60.7	62	63.9	66.5
Time (sec)	0.5	1	1.5	2	2.5	3	3.5	4	4.5	5

The power and duration required to reach 50°C were determined to be 0.3 W and 1 minute.

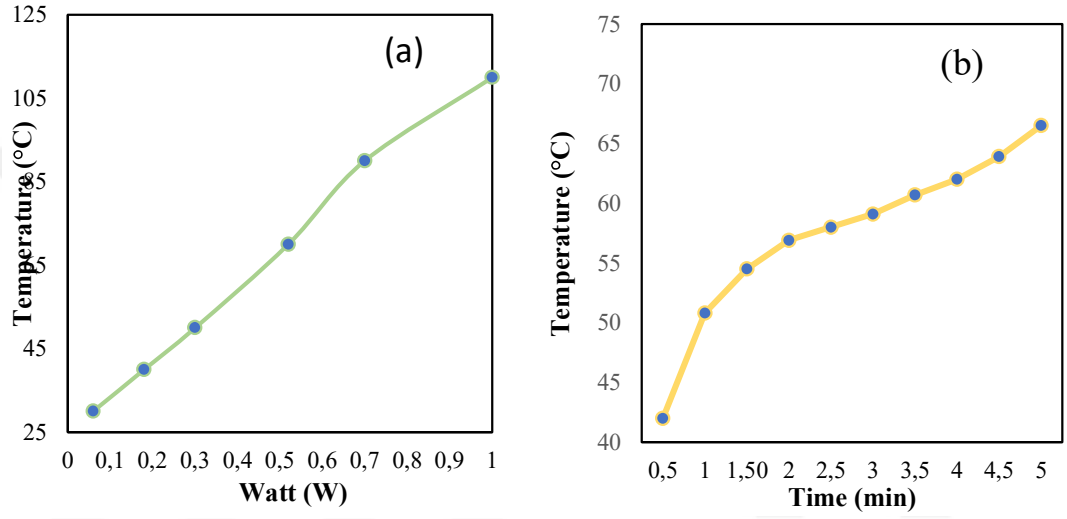

Figure 0.3 (a) Temperature changes with applying power (watt), (b) Temperature changes with time

3.2 Electrochemical Characterization

The CV cleaning proceeded between -0.5 V and 1.75 V until the peaks which were oxidation and reduction, were not switching and after this to determine the cleaning characterization, the electrodes were cycled with CV in the 1 mM ferri/ferrocyanide. CV was characterized to determining peak-to-peak separation between -0.25 V and 0.5 V and EIS results were recorded as charge transfer resistance (R_{CT}). The R_{CT} values were performed pre probe, post probe, and post target measurement in a 1 mM ferri/ferrocyanide solution. The EIS frequencies were changed between 100 kHz and 0.1 Hz.

3.2.1 The Cleaning Performance of Electrodes

Prior to the characterization of the macro-gold electrodes, the cleaning procedure was carried out in several steps; polishing, piranha treatment, and voltage cycling in 0.1 M H_2SO_4, between -0.5 V and 1.75 V about 30 cycles until graph unchanged, as shown in Figure 3.4a. C223AT SPE was characterized cycled in 0.1 M H_2SO_4, between -0.05 V and 1.2 V about 100 cycles until graph unchanged, shown in Figure 3.4b, and cleaning quality was characterized by CVs measurement in 1 mM ferri/ferrocyanide solution which is a redox couple and also can be controlled electron transfer [60, 61].

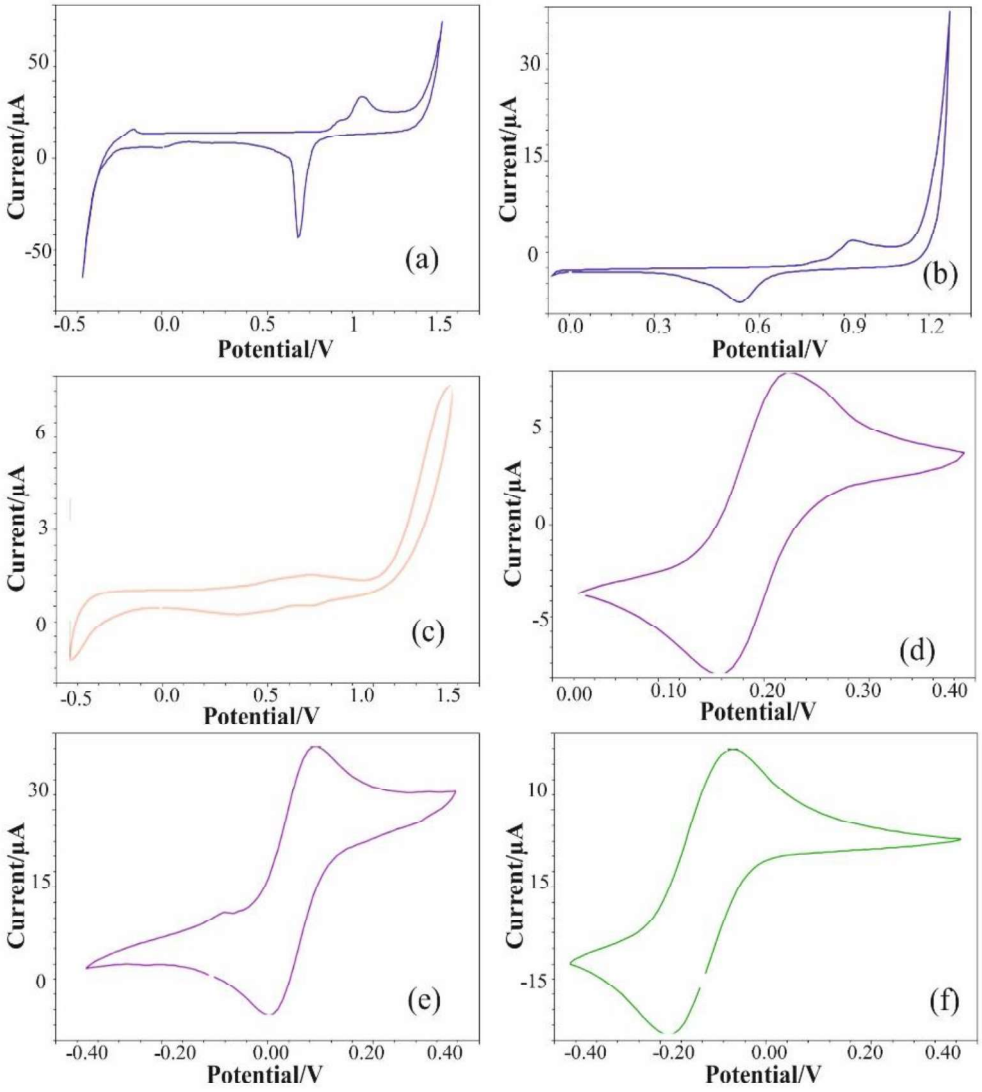

Figure 0.4 CVs of (a) macroelectrode, (b) SPEs, (c) hybrid-chip in 0.1 M H_2SO_4; (d) macroelectrode, (e) SPEs, (f) hybrid-chip in 1 mM FF

Hybrid-chip was cycled in 0.1 M H_2SO_4, between -0.4 V and 1.4 V about 150 cycles until graph unchanging and Figure 3.4c illustrates CVs of hybrid-chip. Peak-to-peak separations were analyzed to characterize electrode cleaning performance. The separation values were calculated 80 mV (Figure 3.4d), 85 mV (Figure 3.4e) and 100 mV (Figure 3.4f) for macro-gold electrode, SPEs and hybrid-chip, respectively. The results are closed to 57 mV which is the ideal value obtained according to the Nernst equation and proves that the cleaning process was successful [19].

3.2.2 Characterization of Surface Functionalization

3.2.2.1 Characterization of Macro-gold Electrode Surface Functionalization

A macro-gold electrode was operated to optimize the experimental procedure. The R_{CT} value which is called pre probe was calculated as 65 Ω (blue curve), and R_{CT} value of after probe was calculated as 389 Ω (red curve). The post target value in which hybridization occurs on the electrode surface was calculated as 687 Ω (green curve) (Figure 3.5a). In Figure 3.5a, the points are the actual values obtained after impedance measurement and the smoothing lines combining these values in the lines. With the correction, the error rate was calculated as 2%.

Increasing R_{CT} values after each treatment showed that probe DNA immobilization and hybridization were successfully performed on the electrode surface. When probe DNA immobilized on the clean electrode surface, inhibited the electron movement of the ferri/ferrocyanide redox pair, and this was recorded as an increase in R_{CT} by the PalmSense device. When target DNA connected to the prop DNA, hybridization blocked the electron transfer, and this caused the R_{CT} value to increase further. Results in Figure 3.5 proves that the probe was attached to the electrode and then hybridization actualized.

Current values decrease after each functionalization steps, as a conclusion these results are compatible with R_{CT} values [62]. The purpose of performed DPV and SWV measurements was to prove the accuracy of increasing resistance with decreasing current. Figure 3.5b and Figure 3.5c demonstrate DPV and SWV graph, the current value decreased after immobilization and hybridization, on the contrary of EIS.

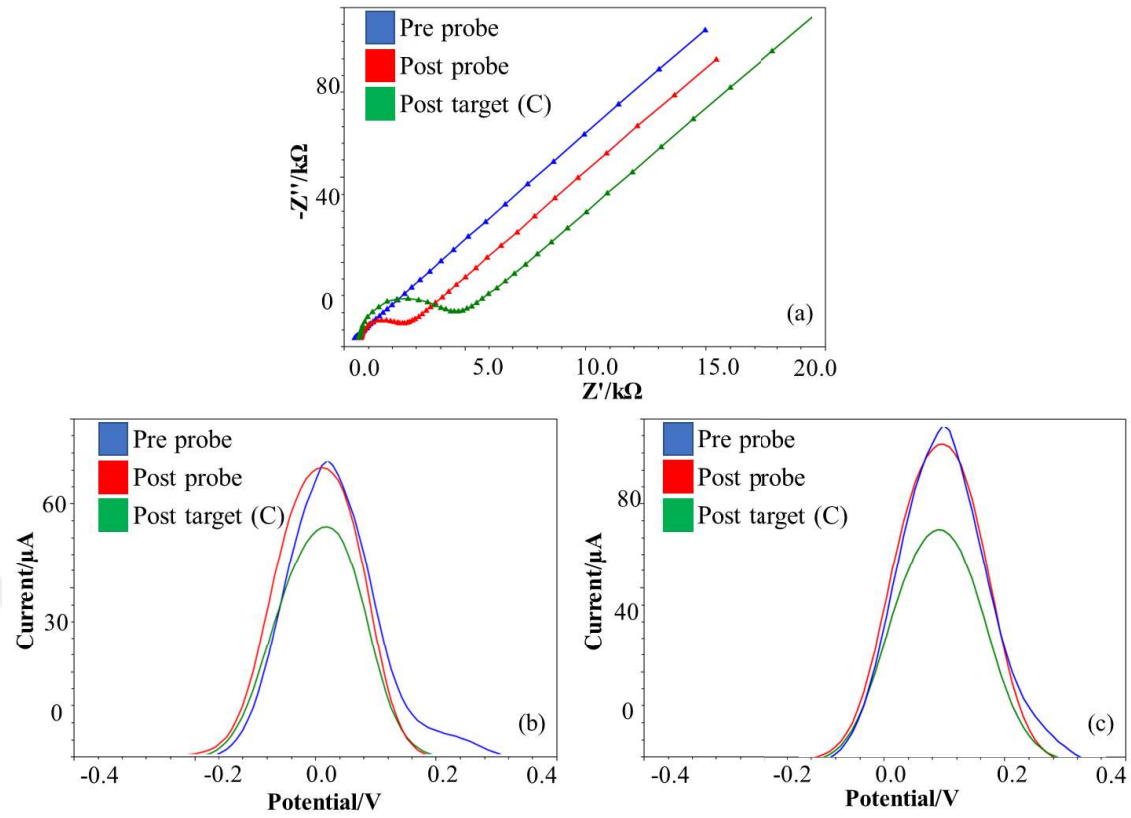

Figure 0.5 EIS results for macro-gold-electrode surface functionalization. (a) Nyquist plot, (b) DPV graph, (c)SWV graph taken in 1 mM ferri/ferrocynide

3.2.2.2 Characterization of the C223AT SPE Surface Functionalization

C223AT SPEs were operated before microelectrode experimental optimization because of their similarity to the microelectrode. At this stage of the study, target hybridization was performed at room temperature (25°C) and 50 °C, complementary target and also non-complementary target sequences which were used to prove selectivity of hybridization, were operated.

Figure 3.6a demonstrates the Nyquist plot of pre probe, post probe, and post target (complementary and non-complementary) measurement of SPE. In Figure 3.6a, the points are the actual values obtained after impedance measurement and the smoothing lines combining these values in the lines. With the correction, the error rate was calculated as 3%.

The R_{CT} results increased after immobilization of probe DNA and complementary target DNA hybridization. R_{CT} values almost unchanged compared to the post probe at the non-complimentary hybridization, because the probe DNA and target DNA didn't match, thence movement of electrons in ferri/ferrocyanide didn't bloke.

DPV and SWV (Figure 3.6b, 3.6c) were performed to control R_{CT} results, as expected the decreasing current value in the complementary target hybridization versus the increasing current value in the non-complementary target hybridization was obtained. As a result, the results obtained by working with SPE prove the successful performance of the experiment.

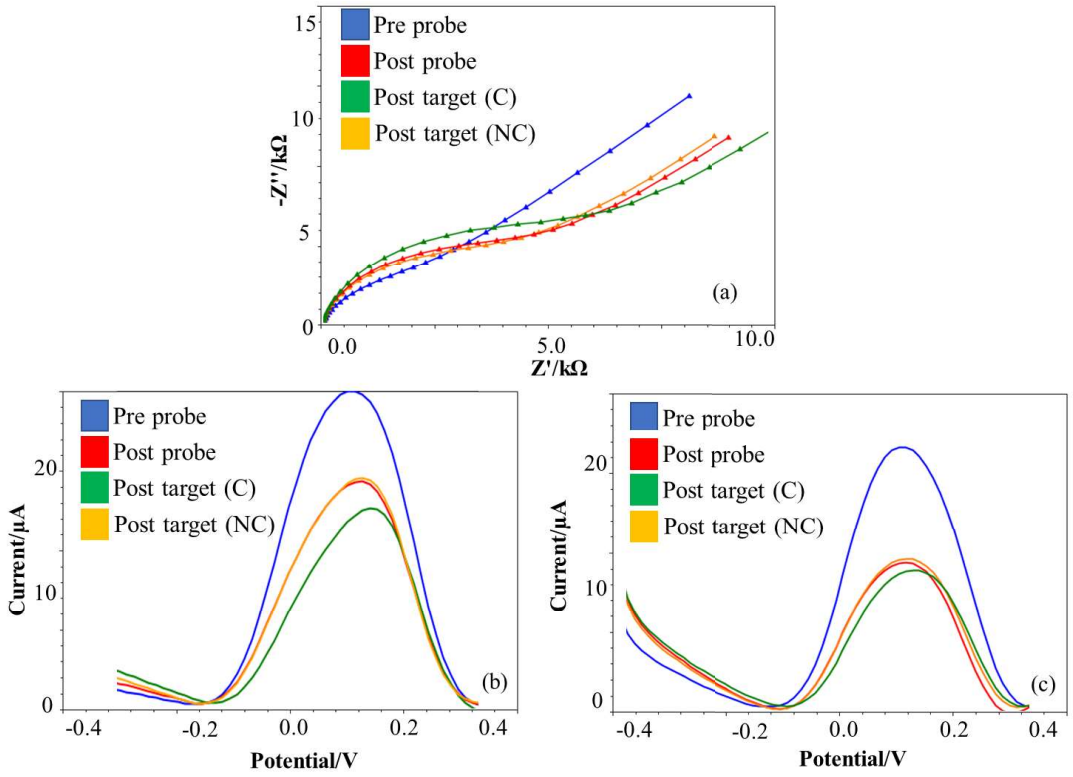

Figure 0.6 EIS results for C223AT SPE surface functionalization. (a) Nyquist plot, (b) DPV graph, (c)SWV graph taken in 1 mM ferri/ferrocynide

Complementary and non-complementary target hybridization was performed at 25°C and 50°C and R_{CT} values were calculated by using PSTrace which is software to PalmSens. The R_{CT} value which is called pre probe was calculated as 2550 Ω, and R_{CT} value of after probe was calculated as 5590 Ω. The complimenatry post target value in

which hybridization occurs on the electrode surface was calculated as 5981 Ω (Figure 3.6a) and also non-complimentary post target value was calculated 5300 Ω. The signal change magnitude was calculated higher in the complementary hybridization at 50°C than in the 25°C (Figure 3.7). Consequently, the probe and target hybridization sensitivity were increased by performing hybridization at a temperature close to the melting temperature. At 25°C and 50°C, the change in the signal amplitude in the hybridization studies performed with the non-complementary target was considerably reduced compared to the obtained with the complementary target. This situation confirms the literature and the results of the experiments have been successful. Apart from these, the increase in hybridization work with the non-complementary target at 25°C is less than from at 50°C. This is due to the high roughness of the electrode surface.

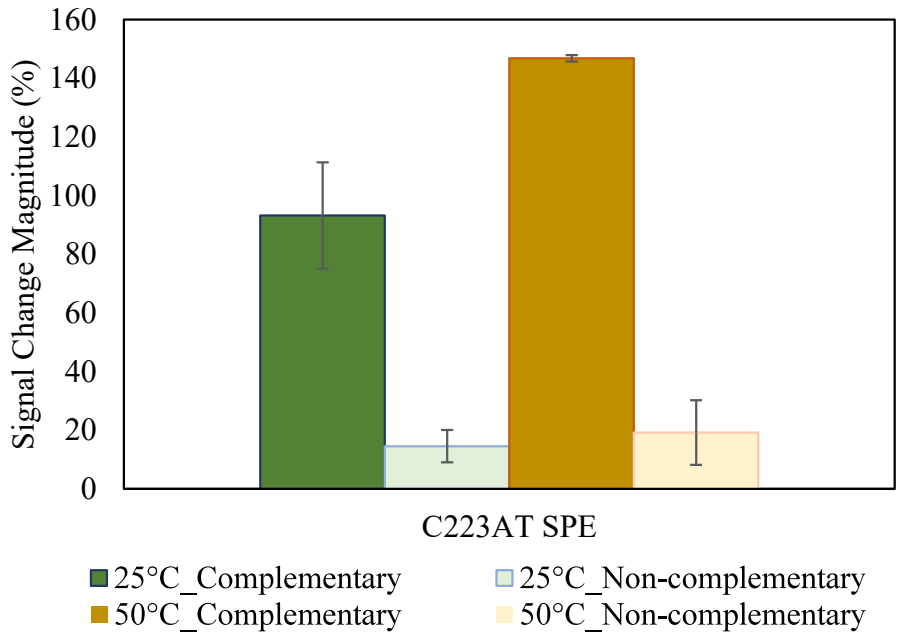

Figure 0.7 Signal change magnitude of post target R_{CT} values for SPEs

3.2.2.3 Characterization of the Hybrid-chip Surface Functionalization

The main purpose of this study was to perform the hybridization process at 50°C using a hybrid-chip where is microheater integrated Au-made microelectrode and to

investigate the performance of the hybrid-chip on EIS experiments. Figure 3.8 illustrates the values obtained in the designed and produced hybrid-chip.

At this stage, the target hybridization process was carried out at 25°C and 50°C, and at the same time, complementary and non-complementary target DNA was used. After the CV cleaning process, the R_{CT} value of the hybrid-chip was measured 197 Ω and then was incubated with probe DNA.

As a result of the immobilization of the probe DNA to the electrode surface, the R_{CT} value was obtained 1114 Ω by fitting Nyquist plot in PSTarce. Finally, a complementary target DNA solution was added to the electrode surface to perform DNA hybridization, and the changing R_{CT} value was calculated as 1498 Ω. The increasing R_{CT} values as a result of each stage prove that the immobilization and hybridization were performed successfully at 25°C.

The hybridization process was carried out by microheater at 50°C and R_{CT} value was calculated as 2785 Ω. Figure 3.8a demonstrates the Nyquist plots of hybrid-chip experiments.

DPV and SWV were performed to control the increase in R_{CT}, as shown in Figure 3.8b and Figure 3.8c. In Figure 3.8a, the points are the actual values obtained after impedance measurement and the smoothing lines combining these values in the lines. With the correction, the error rate was calculated as 3.1%.

Current values decrease after each functionalization steps, as a conclusion these results are compatible with R_{CT} values and thus prove the performance of the experiment.

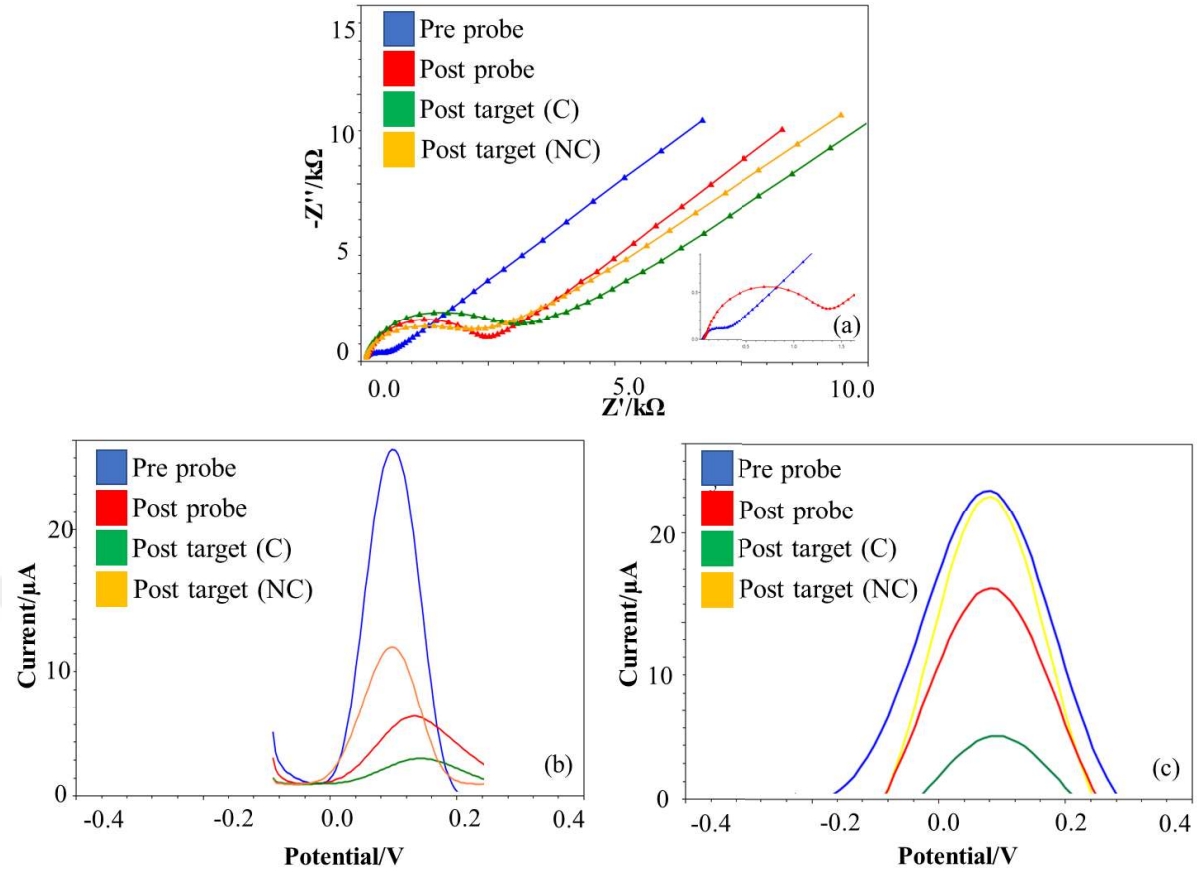

Figure 0.8 EIS results for Au-made microelectrode surface functionalization. (a) Nyquist plot, (b) DPV graph, (c)SWV graph taken in 1 mM ferri/ferrocynide

As a further study, hybridization with the non-complementary target was performed at 25°C and 50 °C. Figure 3.9 illustrates signal change magnitudes which were performed with a complimentary target at 25°C and 50°C, and also demonstrates with the non-complementary target. The results proved that the complementary target DNA hybridized sensitively at both temperatures, but the non-complementary target hybridization didn't actualize precisely.

In the study conducted with a hybrid-chip at 50°C, it is proved with the values in the signal change graph (Figure 3.9) that the hybridization sensitivity increased, and at the same time, the fact that the study was carried out on Au-made microelectrode positively affected the sensitivity of the process. The signal change magnitudes in the studies with the non-complementary target at 25°C and 50°C were calculated as 92% and 66%, respectively.

In this case, non-complementary binding was prevented as a result of structural properties of Au-made microelectrode, and at the same time, the hybridization was performed more sensitive at 50°C by microheater.

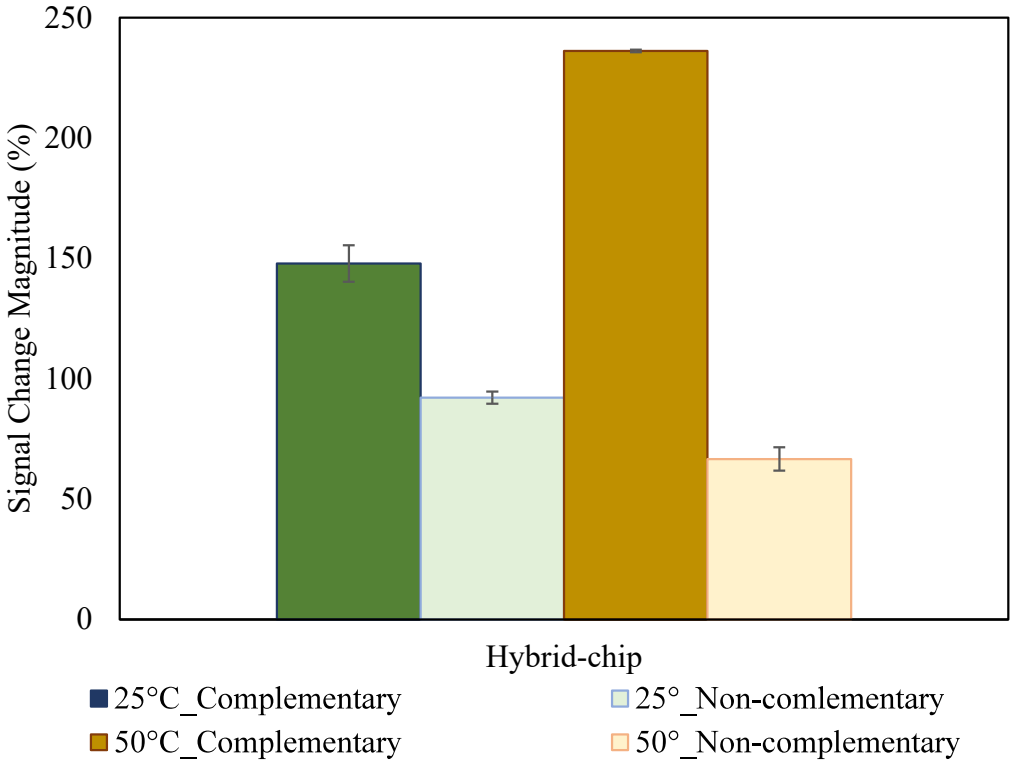

Figure 0.9 Signal change magnitude of post target R_{CT} values for hybrid-chip

At the hybrid-chip system, the non-complementary measurement reached a lower signal change at 50°C as to 25°C, this indicates that temperature improves sensitivity. Therefore, the EIS results with non-complementary target confirm the specificity of the hybrid-chip sensor.

The signal change magnitude of hybrid-chip was higher than that of SPE samples at both temperatures, which is due to the smooth and more defect-free surface of the Au-made microelectrodes and this also caused a lower signal variation for the hybrid-chip.

A two-tailed t-test was performed to compare complementary and non-complementary target hybridization signals. Figure 3.10 illustrates the outcome of the t-test and proves that there were statistically significant differences between the complementary and

non-complementary. This difference was even more enhanced when the incubation was performed at 50°C. Higher signal changes were also observed at 50°C on the SPEs, giving confidence that incubating at higher temperatures improved sensitivity.

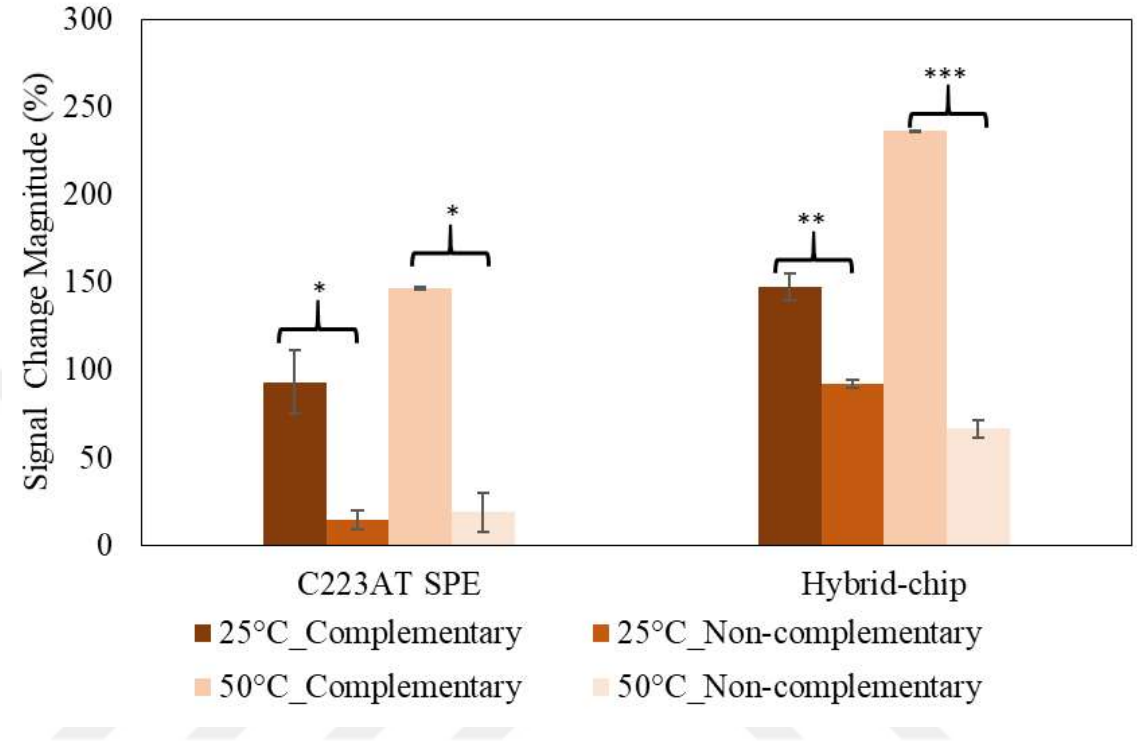

Figure 0.10 Signal change of SPEs (left) and hybrid-chip (right) for the complementary and non-complementary targets at 25°C and 50°C. Error bars represent standard error of the mean (n = 3) and *p≤0.004; **p≤0,003; ***p≤0,0001 represent p-value of t-test

3.2.3 AFM Characterization of Electrodes

After the CV cleaning of the SPEs and Au-made microelectrode, root means square (RMS) values were calculated of 49 µm X 49 µm areas, 172.5 nm, and 7.3 nm for SPEs and hybrid-chip, respectively, shown in Figure 3.11a and Figure 3.10b. This indicates the surface roughness was considerably higher for the SPEs (Figure 3.10a). The difference is a consequence of the rough surface of the SPE, leading to the less controllable formation of the self-assembled monolayer (SAM) with more variable surface coverage than that of the smooth chip which results in the improved performance of the chip in the hybridization experiments with the non-complementary target at 50°C. It is noticed that there are long lines on the surface of the microchip

electrode in the AFM image, shown in Figure 3.11b. The reason for this is that the microchips were cut off with the help of vacuum tape after gold coating. The residue of the vacuum band can be cleaned with acetone, but when the surface of the microchip electrode is exposed to acetone, it has been observed that the gold coating, together with the remnants of the vacuum band, detaches from the surface or becomes thinner part by section.

The AFM images prove that there is an inverse proportion between the surface roughness of the electrodes and the measurement accuracy. Having a higher roughness value than the hybrid-chip electrode, the sensitivity of SPEs is lower. Because the surface roughness affects the immobilization of the probe DNA at maximum performance and increases the error rate [63].

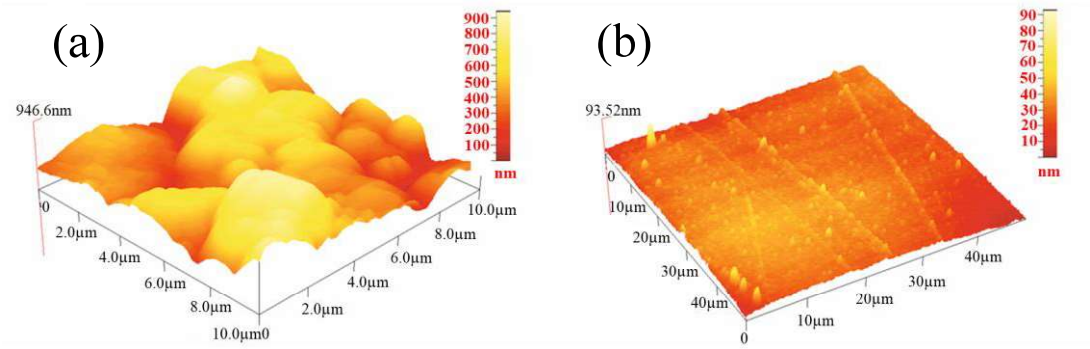

Figure 0.11 Atomic Force Microscopy picture of (a) SPEs (C223AT), (b) Au-made microelectrode (49 µm x 49 µm area)

CHAPTER 4

CONCLUSION

In this study, we present the development of a novel microheater integrated Au-made microelectrode with enhanced DNA hybridization sensitivity based on EIS experiments. The microheater electrode and the EIS electrode were both made of Au deposited on a thin Cr layer on a glass slide through a shadow mask. Production is facile and low cost because the same shadow mask can be used to produce both electrodes and there is no need for any photolithography steps.

The results of the experimental heating tests were in line with the simulations, indicating that power of 0.3 W was sufficient to reach the desired temperature, 50°C, within a minute. Sensitivity was increased by about 50% and 90% when the hybrid chip was used at room temperature and 50°C, respectively, compared to the off-chip experiments. As a result, the hybrid chip operates with a 3% tolerance.

Enhanced sensitivity and selectivity are a result of the surface properties of the electrodes, as shown by AFM images, and most importantly the use of microheater around the electrode.

We believe that the concept of integrated microheater is a novel approach in improving the assay performance in not only EIS-based susceptibility assays as such but also the on-chip biosensors in general. It will also pave the way for the development of a more sophisticated and functional sensor with higher throughput.

4.1 Future Directions

In the light of the experiments and results, with the success of hybridization at 50°C, a microfluidic platform can be integrated on the hybrid-chip to perform functionalizing step completely covered microfluidic chip.

The experiments can be actualized on the gold electrodes obtained as a result of different deposition methods and the effect of the deposition method on the R_{CT} value can be examined.

REFERENCES

[1] Damborský, P., Švitel, J., and Katrlík, J "Optical biosensors," Essays in Biochemistry, 60(1), 91-100, 2016.

[2] Guzel, F. D. & Citak, F., "Development of an on-chip antibiotic permeability assay with single molecule detection capability," IEEE transactions on Nanobioscience, 17(2), 155-160, 2018.

[3] Guzel, F. D. & Avci, H., "Fabrication of nanopores in an ultra-thin polyimide membrane for biomolecule sensing," IEEE Sensors Journal, 18(7), 2641-2646, 2018.

[4] Karunakaran, C., Bhargava, K., and Benjamin, R., Biosensors and bioelectronics, Elsevier, 2015.

[5] Corrigan, D.K., Blair, E. O., Terry, J. G., Walton, A. J., and Mount, A. "Enhanced electroanalysis in lithium potassium eutectic (LKE) using microfabricated square microelectrodes," Analytical Chemistry, 86(22), 11342-11348, 2014.

[6] Mehrotra, P., "Biosensors and their applications–A review," Journal of Oral Biology; Craniofacial Research, 6(2), 153-159, 2016.

[7] Songa, E.A. & Okonkwo, J., "Recent approaches to improving selectivity and sensitivity of enzyme-based biosensors for organophosphorus pesticides: A review," Talanta, 155, 289-304, 2016.

[8] Baranauskas, G., Gusmeroli, R., Spinelli, A. S., Giordano, C., and Raimondi, M. T., "Cell-based biosensors: Current trends of the development", Journal of Applied Biomaterials; Biomechanics, 4(3), 125-134, 2006.

[9] Song, S., Wang, L., Li, J., Fan, C., and Zhao, J., "Aptamer-based biosensors",Trends in Analytical Chemistry, 27(2), 108-117, 2008.

[10] Elgrishi, N., Rountree, K. J., McCarthy, B. D., Rountree, E. S., Eisenhart, T. T., and Dempsey, J. L., "A practical beginner's guide to cyclic voltammetry", Journal of Chemical Education, 95(2), 197-206, 2018.

[11] Park, Y. J. & Park, S. M., "DNA hybridization sensors based on electrochemical impedance spectroscopy as a detection tool", Sensors, 9(12), 9513-9532, 2009.

[12] Yoon, J. T., "Introduction to biosensors: from electric circuits to immunosensors", Springer, 2016.

[13] Nikhil, B., Pawan, J., Nello, F., and Pedro, E., "Introduction to biosensors," Essays in Biochemistry, 60(1), 1-8, 2016.

[14] Malhotra, S., Verma, A., Tyagi, N., and Kumar, V., “Biosensors: principle, types and applications,” International Journal of Advance Research and Innovative Ideas in Education, 3(2), 3639-3644, 2017.

[15] Hoß, S. G. & Bendas, G., "Mass-sensitive biosensor systems to determine the membrane interaction of analytes," Antibiotics, 145-157, Springer, 2017.

[16] Alper, M., “Electrodeposited magnetic superlattices:growth, characterization, magnetic and magnetotransport properties,” University of Bristol, 1995.

[17] Thevenot, D. R., Toth, K., Durst, R. A., and Wilson, G. S., “Electrochemical biosensors: recommended definitions and classification,” Journal of Pure Applied Chemistry, 71(12), 2333-2348, 1999.

[18] Bonanni, A., Fernández-Cuesta, I., Borrisé, X., Pérez-Murano, F., Alegret, S., and del Valle, M., “DNA hybridization detection by electrochemical impedance spectroscopy using interdigitated gold nanoelectrodes,” Journal pf Microchimica Acta, 170(3-4), 275-281, 2010.

[19] Butterworth, A., Blues, E., Williamson, P., Cardona, M., Gray, L., and Corrigan, D. K., “SAM composition and electrode roughness affect performance of a DNA biosensor for antibiotic resistance,” Journal of Biosensors, 9(1), 22, 2019.

[20] Peng, H. P., Hu, Y., Liu, P., Deng, Y-N, Wang, P., Chen, W., Liu, A-L., Chen, Y-Z, and Lin, X-H,“Label-free electrochemical DNA biosensor for rapid detection of mutidrug resistance gene based on Au nanoparticles/toluidine blue–graphene oxide nanocomposites,” Sensors and Actuators B: Chemical, 207, 269-276, 2015.

[21] Fojta, M., “Detecting DNA hybridization and damage,” Analytical Chemistry, 73(3), 74A, 2001.

[22] Macdonald, D., “Reflections on the history of electrochemical impedance spectroscopy,” Electrochimica Acta, 51(8-9), 1376-1388, 2006.

[23] Lisdat,F. & Schäfer, D., “The use of electrochemical impedance spectroscopy for biosensing,”Analytical; Bioanalytical Chemistry, 391(5), 1555, 2008.

[24] Macdonald, D., “A brief history of electrochemical impedance spectroscopy,”Journal of the Electrochemical Society, 2020, 72-88, 2002.

[25] Macdonald, J. R., “Impedance spectroscopy,” Anals of Biomedical Engineering, 20(3), 289-305, 1992.

[26] Blair, E. O., Hannah, S., Vezza, V., Avcı, H., Kocagoz, T., Hoskisson, P. A., Güzel, F. D., and Corrigan, D. K., “Biologically modified microelectrode sensors provide enhanced sensitivity for detection of nucleic acid sequences from Mycobacterium tuberculosis,” Sensors and Actuators Reports, 100008, 2020.

[27] Saiki, R. K., Gelfand, D. H., Stoffel, S., Scharf, S. J., Higuchi, R., Horn, G. T., Mullis, K. B., and Erlich, H. "Primer-directed enzymatic amplification of DNA with a thermostable DNA polymerase," Journal of Science, 239(4839), 487-491, 1988.

[28] Putra, L. A. G., Yonathan, C. I., Niedhatrata, N. I., Firdaus, M. H. R., and Yoewono, J. R., "A review of the development of Polymerase Chain Reaction technique and its uses in Scientific field," Stannum: Jurnal Sains dan Terapan Kimia, 2(1), 14-30, 2020.

[29] Damiati, S., Haslam, C., Søpstad, S., Peacock, M., Whitley, T., Davey, P., and Awan, S. A., "Sensitivity Comparison of Macro-and Micro-electrochemical Biosensors for Human Chorionic Gonadotropin Biomarker Detection," IEEE Acsess, 7, 2019.

[30] Zhang, D. Y., Chen, S. X., and Yin, P. J. "Optimizing the specificity of nucleic acid hybridization," Nature Chemistry, 4(3), 208-214, 2012.

[31] Guruviah, V., "Design of microheaters with better thermal management for sensor applications", International Journal of Mechanical Engineering and Technology,8(10), 823-828, 2017.

[32] Zhang, K. L., Chou, S. K., and Ang, S. S., "Fabrication, modeling and testing of a thin film Au/Ti microheater", International Journal of Themral Sciences, 46(6), 580-588, 2007.

[33] Phatthanakun, R., Deekla, P., Pummara, W., Sriphung, C., Pantong, C., and Chomnawang, N., "Design and fabrication of thin-film aluminum microheater and nickel temperature sensor", 2012 7th IEEE International Conference on Nano/Micro Engineered and Molecular Systems (NEMS), 112-115.

[34] Tiggelaar, R. M., "Silicon-technology based microreactors for high-temperature heterogeneous partial oxidation reactions", MS Thesis, University of Twente, Enschede, The Netherlands, 2004.

[35] Spruit, R. G., Van Omme, J. T., Ghatkesar, M. K., and Garza, H. P., "A Review on Development and Optimization of Microheaters for High-TemperatureIn SituStudies", Journal of Microelectromechanical Systems, 26(6),1165-1182, 2017.

[36] Chang, W. Y., & Hsihe, Y. S., "Multilayer microheater based on glass substrate using MEMS technology," Microelectronic Engineering, 149,25-30, 2016.

[37] Simon, I., Bârsan, N., Bauer, M., and Weimar, U., "Micromachined metal oxide gas sensors: opportunities to improve sensor performance" Sensors Actuators B: Chemical, 73(1), 1-26, 2001.

[38] VanHorn, A., & Zhou, W., "Design and optimization of a high temperature microheater for inkjet deposition", The International Journal of Advanced Manufacturing Technology, 86(9-12), 3101-3111, 2016.

[39] Bedoui, S., Gomri, S., Samet, H., and Kachouri, A., "Design and electro-thermal analysis of a platinum micro heater for gas sensors", 2016 13th International Multi-Conference on Systems, Signals & Devices (SSD), 558-561.

[40] Sidek, O., Ishak, M., Khalid, M., Bakar, M. A., and Miskam, M., "Effect of heater geometry on the high temperature distribution on a MEMS micro-hotplate", 2011 3rd Asia Symposium on Quality Electronic Design (ASQED), 100-104.

[41] Shah, K. S., Gupta, S. R., Dalvi, G. V., Rathod, S. S., and Kasambe, P. V., "Performance Analysis of MEMS Microheater by Optimizing Coıl Design Using Coventorware", Journal of Research in Engineering and Applied Sciences, 1(3), 135-140, 2016.

[42] Bhowmick, S., Iodice, M., Gioffrè, M., Breglio, G., Irace, A., Riccio, M., Romano, G., Grilli, S., Ferraro, P., and Mecozzi, S., "Investigation of pyroelectric fields generated by lithium niobate crystals through integrated microheaters," Sensors Actuators A: Pysical, 261, 140-150, 2017.

[43] Coppola, G., Striano, V., Ferraro, P., De Nicola, S., Finizio, A., Pierattini, G., and Maccagnani, P., "A nondestructive dynamic characterization of a microheater through digital holographic microscopy," Journal of microelectromechanical systems, 16(3), 659-667, 2007.

[44] Ahmed, A., Baskaran, F., Rabih, A. A., Dennis, J., Khir, M. M., and Elmaleeh, M. A., "Design, Modeling and Simulation of Microhotplate for Application in Gas Detection." 2018 International Conference on Intelligent and Advanced System (ICIAS),1-5,2018.

[45] S. Z. Ali, F. Udrea, W. I. Milne, and J. W. Gardner, "Tungsten-based SOI microhotplates for smart gas sensors," vol. 17, no. 6, pp. 1408-1417, 2008.

[46] Noor, M. M., Sugandi, G., Aziz, M. F., and Majlis, B. Y., "Effects of material and membrane structure on maximum temperature of microheater for gas sensor applications", 2014 IEEE International Conference on Semiconductor Electronics (ICSE2014), 255-258. 2014.

[47] Holt, N., Marques, L. G., Van Horn, A., Montazeri, M., and Zhou, W., "Fabrication and control of a microheater array for Microheater Array Powder Sintering", The International Journal of Advanced Manufacturing Technology, 95(1-4), 1369-1376, 2018.

[48] Bhattacharyya, P., "Technological journey towards reliable microheater development for MEMS gas sensors: A review," IEEE Transactions on Device Materials Reliability, 14(2), 589-599, 2014.

[49] Puigcorbe, J., Vogel, D., Michel, B., Vila, A., Gracia, I., Cane, C., and Morante, J. R., “Thermal and mechanical analysis of micromachined gas sensors,” Journal of Micromechanics Microengineering, 13(5), 548, 2003.

[50] Guo, B., Bermak, A., Chan, P. C., and Yan, G.-Z., “An integrated surface micromachined convex microhotplate structure for tin oxide gas sensor array,” IEEE Sensors Journal, 7(12), 1720-1726, 2007.

[51] Pineault, N., Robert, A., Cortin, V., and Boyer, L., "Ex vivo differentiation of cord blood stem cells into megakaryocytes and platelets," Basic Cell Culture Protocols, 205-224, Springer, 2013.

[52] Spannhake, J., Helwig, A., Müller, G., Faglia, G., Sberveglieri, G., Doll, T., Wassner, T., and Eickhoff, M. “SnO2: Sb–A new material for high-temperature MEMS heater applications: Performance and limitations,” Sensors Actuators B: Chemical, 124(2), 421-428, 2007.

[53] Toskov, S., Glatz, R., Miskovic, G., and Radosavljevic, G., "Modeling and fabrication of pt micro-heaters built on alumina substrate." Proceedings of the 36th International Spring Seminar on Electronics Technology, 47-52, 2013.

[54] Kups, T., Hotovy, I., and Spieß, L., "TEM investigation of sputtered indium oxide layers on silicon substrate for gas sensors." EMC 2008 14th European Microscopy Congress 1–5 September 2008, Aachen, Germany, 345-346, 2008.

[55] Ha, S-M., Cho, W., Ahn, Y., and Hwang, S. Y., “An integrated microfluidic device for rapid cell lysis and DNA purification of epithelial cell samples,” Journal of Nanoscience Nanotechnology, 11(5), 4250-4253, 2011.

[56] Li, S., & Chen, S.,“Design, simulation, and microfabrication of a heat-conduction DNA chip with integrated microheaters,” Journal of manufacturing processes, 6(1), 81-87, 2004.

[57] Nieto, D., McGlynn, P., De La Fuente, M., Lopez-Lopez, R., and O’connor, G., “Laser microfabrication of a microheater chip for cell culture outside a cell incubator,” Colloids Surfaces B: Biointerfaces, 154, 263-269, 2017.

[58] Javed, A., Iqbal, S. M., and Jain, A., “Microheater platform for selective detachment of DNA,” Applied Physics Letters, 101(9), 093707, 2012.

[59] Markegard, C. B., Gallivan, C. P., Cheng, D. D., and Nguyen, H. D., “Effects of concentration and temperature on DNA hybridization by two closely related sequences via large-scale coarse-grained simulations,” The Journal of Physical Chemistry B, 120(32), 7795-7806, 2016.

[60] Randviir, E. P., and Banks, C. E., “Electrochemical impedance spectroscopy: an overview of bioanalytical applications,” Analytical Methods, 5(5), 1098-1115, 2013.

[61] Horvat-Radošević, V, Kvastek, K., and Križekar, D., “Kinetics of the [Fe (CN) 6] 3-/[Fe (CN) 6] 4-Redox Couple Reaction on Anodically Passivated Fe 80 B 20,”Chorta Chemial Acta, 70(2), 537-561, 1997.

[62] Gupta, M. S., “Georg Simon Ohm and Ohm's Law,” IEEE Transactions on Education, 23(3), 156-162, 1980.

[63] Wang, X., Lai, W., Man, T., Qu, X., Li, L., Chandrasekaran, A. R., and Pei, H., “Bio-surface engineering with DNA scaffolds for theranostic applications,” Nanofabrication, 4(1), 1-16, 2018.